Impact of heatwaves and system shocks on a nearly zero energy educational building: Is it resilient to overheating?

Abantika Sengupta[†]*[1], Douaa Al Assaad[†1], Josué Borrajo Bastero[2], Marijke Steeman[2], Hilde Breesch[1]

[1]KU Leuven, Department of Civil Engineering, Building Physics and Sustainable Design, Ghent Campus, Gebroeders De Smetstraat 1, 9000 Gent, Belgium.

[2]Ghent University, Department of Architecture and Urban Planning, Jozef Plateaustraat 22 9000 Gent, Belgium.

*Corresponding author: Abantika Sengupta (E-mail: abantika.sengupta@kuleuven.be), 032485598043

[†]*The authors contributed to this manuscript equally*

Abstract

The characteristic that describes the extent to which buildings and their systems maintain their performance during *shocks* is called *resilience*. Building policies in the EU have already addressed the resilience of buildings against possible hazards (i.e., natural disasters, extreme weathers, fires). However, with increasing overheating risks (e.g., climate change) accompanied by their detrimental health and economic impacts, the thermal performance of nearly zero energy buildings (nZEB) is not guaranteed. This study aims to assess the impact of shocks and combinations on the *thermal resilience* of educational nZEB against heatwaves (*HW*) and system shocks (*SS*) including failure of indirect evaporative cooling (*IEC*), natural night ventilation (*NNV*) and solar shading failure (*SF*). A Modelica model of the building was developed and experimentally validated. Shocks were classified and quantified using the *novel normalized degree of shock (doS)* index. **Heatwaves** (**HWs**) had 20× to 93× more critical impact than the worst **SS (NNV failure).** Additionally **SS** occurring at the start of the operational period is 1.2× more critical than **SS** occurring later in the day as it allowed for

significant heat build-up in both classrooms. In future climate scenarios a combination of **HWs** and **power outages** will become frequent. This study showed that a combination of a full day of cooling strategy and shading failure occurring on the hottest day of a 6-day long **HW**, is 10% more critical on both lecture rooms than an individual 10-day long **HW**. Classroom with heavy thermal mass prolongs the absorptivity of the shocks but delays recovery.

Keywords

Passive cooling strategies, educational building, thermal resilience, overheating, degree of shock

Nomenclature

ACF	Air conditioning failure
AHU	Air handling unit
BMS	Building monitoring system
DCV	Demand-controlled ventilation
doS	Normalized Degree of shock (-)
$doES$	Normalized Degree of external shock (-)
$doSS$	Normalized Degree of system shock (-)
ES	External Shock
ESF	Envelope strategy failure
HVAC	Heating ventilation and air conditioning
HW	Heat wave
IDEAS	Integrated district energy assessment by simulation
IEC	Indirect evaporative cooling
nZEB	Nearly zero energy building
NNV	Natural night ventilation

NS	No shock
PI	Proportional integral
PO	Power outage
RH	Relative humidity (%)
SF	Shading Failure
SS	System shock
T	Temperature
t	time (h)
TLR	Test lecture room
TMY	Typical meteorological year
$\overline{T_{oa,ES}}$	Average outdoor dry bulb temperature during external shock (℃)
$\overline{T_{oa,TMY}}$	Average outdoor dry bulb temperature during typical meteorological year (℃)
$\overline{T_{ra,NS}}$	Average zone air temperature during no shock (℃)
$\overline{T_{ra,VF}}$	Average zone air temperature during ventilation failure (℃)
$\overline{T_{sa,CSF}}$	Average supply air temperature during cooling system failure (℃)
$\overline{T_{sa,NS}}$	Average supply air temperature during no shock (℃)
$\overline{T_{wn,NS}}$	Average window internal surface temperature during no shock (℃)
$\overline{T_{wn,SF}}$	Average window internal surface temperature during shading failure (℃)
t_{op}	Total operational hours of the system in one day (h)
t_{shock}	Shock duration (h)
VAV	Variable air volume
VF	Ventilation failure

Greek symbols

ρ	Density (kg/m^3)
η	Efficiency (%)

Subscripts

a	air
avg	average
oa	outdoor air
op	operational (without any shock/interruption)
max	maximum
min	minimum
ra	room air
sa	supply air
wn	window

1. Introduction

Heating, Ventilation and Air conditioning (HVAC) systems are installed in buildings to provide occupants with good levels of thermal comfort during cooling and heating seasons. This is essential to maintain their wellbeing and productivity. In educational buildings, students spend considerable amounts of time in classrooms. Providing them with comfortable indoor conditions is crucial for their cognitive development and academic performance [1,2]. However, this process is energy intensive given the high occupancy loads and glazing ratios often found in educational buildings [3]. This increases their carbon footprint, further contributing to the worsening climate change conditions [4]. Thus, globally, and especially in the EU, a shift towards designing energy efficient buildings was put in motion through revision of building codes and standards [5,6].

Energy efficient year-round solutions include having highly insulated and airtight envelopes [7,8], improved glazing [9], and solar shading [10]. During the cooling season, passive cooling systems were installed, such as ground source cooling [11], natural night ventilation (NNV) [12] and evaporative cooling [13]. The main goal of any energy efficient building is to meet thermal comfort needs at reduced energy costs [14]. Balaras et al. [8] showed that well-insulated and air-tight buildings in Greece have 20-40% less energy use compared to non-insulated leaky buildings. A simulation study [10] evaluating the performance of solar shading in offices in several climates reduced energy use by 5 to 77%. The research of Becker et al. [15] and Heracleous et al. [16] in educational buildings in Europe demonstrated 18%-33% energy savings by additionally implementing NNV. Harrouz et al. [17] found that dew point evaporative cooling achieved 70% savings in energy costs as compared to active air conditioning in classrooms.

While these buildings and their systems succeed in providing energy-efficient comfortable environments, they are still designed under expected weather and operational

conditions (i.e., occupancy loads, solar heat gains, etc.), which is not always the case. Throughout their lifetime, buildings can be faced with sudden shocks and unforeseen events, that cause the indoor thermal environment to deviate from the designed comfort conditions by causing over or underheating [18,19], impacting occupants' health [20,21]. Underheating causes hypothermia, decreased metabolic activity and cardiovascular stress [22]. Overheating increases human body core temperature impacting basic bodily functions. This not only affects the wellbeing of occupants, but increases mortality rates (heat-strokes) [23]. Overheating is a concern in the EU which is witnessing warmer and longer summers [24] with the incidence of severe heatwaves, lasting from a few days to several weeks, with weather forecasts predicting an increase in their frequency and severity [25]. This puts extreme pressure on the electric grid and thus, heatwaves are often accompanied by power outages further exacerbating overheating [26,27]. In July 2019, Europe experienced historical records for highest temperatures [28], with 2,964 associated deaths in the Netherlands [29]. Severe heatwaves will become the norm by 2050, which could lead to a 257% increase in heat-related mortality in vulnerable communities [25]. In addition, buildings can face other shocks related to failure in system operation. This includes failure of air conditioning [30] and envelope strategies [31], which lead to indoor overheating during the cooling season. Systems' failure is a common occurrence in buildings especially with increasing system complexity. It can be due to faulty sensors, failure or absence of efficient fault diagnostics techniques and poor or irregular maintenance [32–34].

While buildings with airtight and highly insulated envelopes delay the onset of overheating, they can delay recovery and create loads that cannot be completely removed by the passive cooling strategies [35]. The extent to which buildings and their systems can withstand shocks, and recover back to the original designed performance, is termed as "thermal resilience" [19]. Therefore, apart from being energy efficient, buildings should also be thermally resilient. The resilient performance of buildings has been assessed and improved

against certain types of shocks with policies set in motion by building legislations. This includes frameworks to improve resilience of new and existing buildings against natural disasters (earthquakes, extreme weather) through quantifying risks and adopting mitigating strategies (e.g., advanced construction materials, damping mechanisms) [36,37]. Building resilience has also been assessed and improved against fire hazards (i.e., fire-resisting materials, water and power backups) [38,39]. As for the field of thermal resilience, the latter has recently gained exposure due to the relevance of overheating risks and their detrimental impact on human health. However, assessment frameworks to quantify shocks and improve buildings' thermal resilience are still lacking.

A few studies have attempted to evaluate qualitatively and quantitatively the thermal resilience of buildings to overheating. IEA EBC's Annex 80 [40] conducted several studies evaluating the thermal resilience of existing buildings and passive cooling strategies [37–40]. Ji et al. [42] evaluated the thermal resilience against a heatwave of a naturally ventilated care facility with interior blinds. They found that simultaneously increasing window opening area size, replacing blinds with external shading, applying green roofs and NNV, can improve the buildings' thermal resilience. Sengupta et al. [44] evaluated the thermal resilience of a Belgian dwelling during the heatwave of 2020 with and without NNV. Their results showed that with implementation of NNV, the building recover 90% faster from the heatwave and decreases maximum temperatures indoors by 4.3°C compared to the building without NNV. While these studies focused on only one type of shocks (heatwaves), they did not evaluate other types of shocks, such as system failures and compare their overheating effects. They also did not test and compare different combinations of these shocks (e.g., heatwaves and power outages) [27,45]. Moreover, the buildings were only equipped with natural ventilation and envelope strategies (e.g., solar shading). Thus, thermal resilience performance of passive cooling strategies (e.g., indirect evaporative cooling) still needs to be assessed. To the authors'

knowledge, no research has been done to classify, quantify and compare the impact on different shock types on the resilience to overheating in buildings.

The aim of this work is to assess the impact of the shocks (i.e., heatwaves, system shocks and combinations) on the thermal resilience performance to overheating of an existing nearly zero energy building (nZEB) in Belgium. It is a very airtight, highly insulated educational building equipped with indirect evaporative cooling (IEC), natural night ventilation (NNV) and automated shading. The paper is organized as follows. Section 2 presents a novel way of classifying shocks and introduces the normalized degree of shock index to quantify them. Section 3 describes the case study building, the corresponding Modelica model and the experimental methodology used for validation [46] as well as the simulation scenarios of shocks. Section 4 presents the obtained results and discussion. Section 5 concludes the current work followed by the study limitations and outlook in section 6. This study will give insight on the level of preparedness of today's nZEB in facing extreme events and is the first step towards a holistic quantitative assessment framework for the thermal resilience performance of buildings.

2. Shocks' classification and quantification

A shock is defined as a sudden disturbance that causes the building to shift partially or completely from its designed conditions for a certain amount of time. Thus, it challenges the resilience performance of buildings [47]. **Figure. 1** illustrates the temporal evolution of temperature during a shock and the different aspects of thermal resilience [19,47]. When the shock occurs, the indoor temperature rises to T_{max}, causing certain levels of discomfort [48,49]. The period during which the temperature rises to T_{max} is denoted as shock **absorptivity time** (t_2-t_1). When the shock ends and/or an employed recovery action becomes effective, the building recovers from this shock back to eventually thermally comfortable levels [20]. This

period is denoted as **recovery time** of the shock (t_3-t_2). The **absorptivity**, **recovery time** and T_{max} depend on several factors:

(1) Type of shock, severity and duration

(2) Building characteristics (e.g., thermal mass, insulation, airtightness, glazing ratio, space volume etc.).

(3) Heating ventilation and air conditioning systems, their control strategies

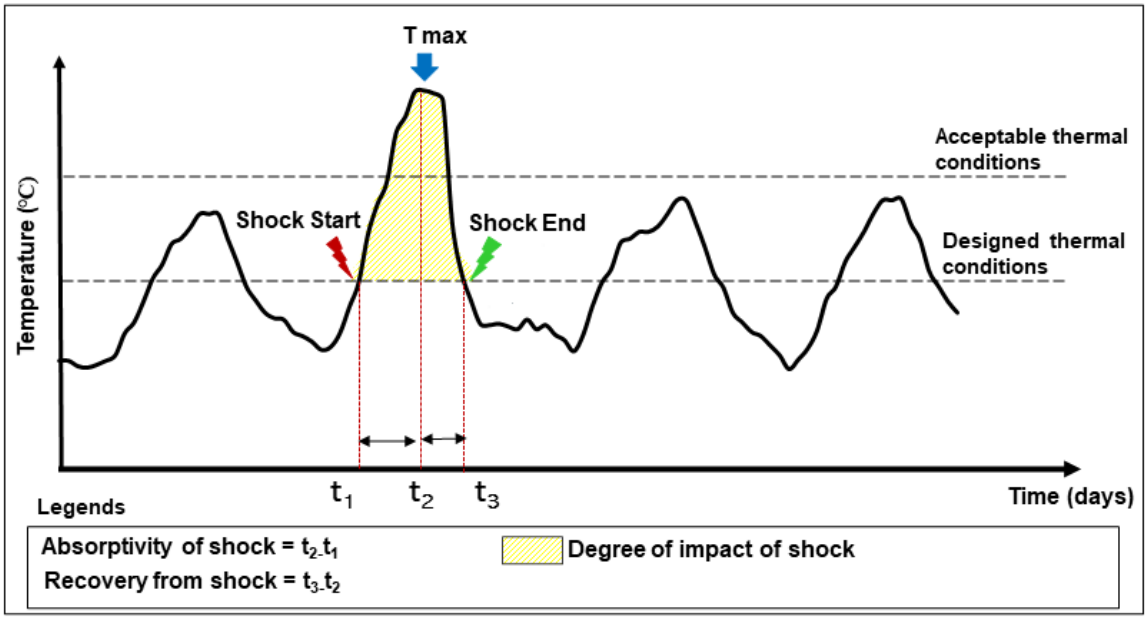

Fig. 1. Temporal evolution of indoor temperature during a shock

To assess and compare the impact of shocks and combinations on the thermal resilience of a building, it is crucial to define, classify and quantify different shocks. Shocks were classified depending on how they impact the thermal environment as will be seen below. To quantify them, this study introduces the normalized degree of shock (doS) index in equation (1):

$$doS = \underbrace{\frac{T_{shock}-T_{ref}}{T_{ref}}}_{\textbf{\textit{Severity}}} \times \underbrace{\frac{t_{shock}}{t_{ref}}}_{\textbf{\textit{Duration}}} \qquad (1)$$

The doS combines the severity and duration of the shock. The aspect of shock severity expressed in equation (1) is a quantification of the shock origin and overheating causality rather than a quantification of shock consequence on the room air temperature, which can be

influenced by multiple parameters simultaneously and not just the shock. Thus, severity is the increase of a shock characteristic temperature T_{shock} compared to the reference characteristic temperature T_{ref} under normal expected conditions. The characteristic temperatures depend on the type of shock. The duration is the ratio of t_{shock} (i.e., the duration of the shock (h) during an observation period ($t_2 - t_1$); (**Fig. 1**) and t_{ref} (i.e., a reference period depending on the type of shock). Two types of shocks were identified as follows:

(1) **External shocks (ES)**: **ES** are events occurring outside the building and cause a significant temporary increase in the outdoor temperatures averaged over t_{shock} ($\overline{T_{oa,ES}}$) compared to typical meteorological year (TMY) temperatures averaged over the same period ($\overline{T_{oa,TMY}}$). **ES** cause overheating by increasing the heat gains through the building envelope (i.e., walls and glazing) and reducing the efficiency of mechanical and ventilative cooling strategies (e.g., evaporative cooling that relies on outdoor wet and dew point temperatures, natural ventilation that relies on outdoor dry bulb temperatures and diurnal temperature differences). **ES** include climate change events such as heatwaves (**HW**) [29], and disaster events (e.g., nearby fire increasing temperatures near the building) [50]. **ES** was quantified by the normalized degree of **ES (**$doES$), defined by equation (2):

$$doES = \underbrace{\frac{\overline{T_{oa,ES}} - \overline{T_{oa,TMY}}}{\overline{T_{oa,TMY}}}}_{\boldsymbol{Severity}} \times \underbrace{\frac{t_{shock}}{t_{shock,max}}}_{\boldsymbol{Duration}} \qquad (2)$$

In (2), $t_{shock,max}$ is the duration of the longest **ES** that is predicted to possibly occur. **ES** can last from a few hours to multiple days.

Note that the $\boldsymbol{doES}$ can be applied to both overheating events due to heatwaves but also underheating events due to cold snaps. ES can be applied to any type of climate zone with knowledge of the meteorological data for the reference case (TMY) and shock case from a weather station or a weather data prediction model.

(2) **System shocks (SS)**: **SS** are partial or complete failure in the operation of building systems in managing the space cooling loads through the envelope or by relying on a working fluid (i.e., air, water). They occur due to faulty feedback sensors in case of automated systems [33], deterioration of components (e.g., motors, valves, dampers, belts) [51], irregular preventive maintenance [52] and inadequate fault detection diagnostics [34]. Depending on the nature of the impaired system, **SS** can cause overheating differently. In this study, three sub-types of **SS** were identified:

I- Envelope strategy failure (ESF) is a failure of any active envelope strategies. This includes any type of external or internal shading failure (**SF**),failure of window cooling in a solar chimney) causing an increase in the solar heat gains through the envelope. Thus, the average internal window surface temperature over t_{shock} during **ESF** ($\overline{T_{wn,ESF}}$) increases with respect to the average internal window surface temperature over the same period ($\overline{T_{wn,NS}}$) in the case of no shock (**NS**). **ESF** shocks can be quantified by $doSS_{ESF}$ in equation (3):

$$doSS_{ESF} = \underbrace{\frac{\overline{T_{wn,ESF}} - \overline{T_{wn,NS}}}{\overline{T_{wn,NS}}}}_{\boldsymbol{Severity}} \times \underbrace{\frac{t_{shock}}{t_{op}}}_{\boldsymbol{Duration}} \qquad (3)$$

In (3), t_{op} refers to the designed operation time of the system.

Note ESF can cause underheating (e.g., failure of window heating using electric strips). The $doSS_{ESF}$ can still be applied in that case. The $doSS_{ESF}$ cannot be applied to fixed envelope elements (i.e., insulation, glazing) as the latter cannot be associated with a failure.

II- Cooling system failure (CSF) (passive or active) installed in a building's air handling unit (AHU). Such failures (i.e., partial, or complete failure of fans, sensor failures, disruption in pumps and water supply) may lead to incomplete or lack of cooling of the characteristic fluid *cf* that drives the cooling load removal from a zone. This leads to an increase in its average temperature over t_{shock} ($\overline{T_{cf,CSF}}$) compared to its average supply temperature for **NS** ($\overline{T_{cf,NS}}$). **CSF** can be quantified by $doSS_{CSF}$ in equation (4):

$$doSS_{CSF} = \underbrace{\frac{\overline{T_{cf,CSF}} - \overline{T_{cf,NS}}}{\overline{T_{cf,NS}}}}_{\textbf{Severity}} \times \underbrace{\frac{t_{shock}}{t_{op}}}_{\textbf{Duration}} \qquad (4)$$

The $doSS_{CSF}$ can be applied to any cooling system including all-air cooling systems (i.e., adiabatic coolers, split air conditioning units, fan coil units and chillers) and hydronic systems (i.e., chilled ceilings, beams). In the case of all-air systems, the cooling fluid is the supplied air *sa* to a zone ($\overline{T_{cf}}$ = $\overline{T_{sa,}}$) while for hydronic systems, the cooling fluid is the supplied water *sw* ($\overline{T_{cf}}$ = $\overline{T_{sw}}$). System failure can also be associated with failure of a heating system causing underheating events (e.g., all-air heating systems such as AHU with heating coils, hydronic heating systems (radiators, heated floors). Equation (4) is still applicable.

III- Ventilation system failure (VF): This includes failure of both natural day ventilation and/or **NNV** through automated windows and failure of a mechanical ventilation system (i.e., partial or complete failure of fans). These strategies provide cooling through supply of outside air. The resulting average room temperature over t_{shock} ($\overline{T_{ra,VF}}$) during the system operation times would be higher than in the case of **NS** ($\overline{T_{ra,NS}}$) . **VF** can be quantified by $doSS_{VF}$ in equation (5):

$$doSS_{VF} = \underbrace{\frac{\overline{T_{ra,VF}} - \overline{T_{ra,NS}}}{\overline{T_{ra,NS}}}}_{\textbf{Severity}} \times \underbrace{\frac{t_{shock}}{t_{op}}}_{\textbf{Duration}} \qquad (5)$$

The $doSS_{VF}$ can be applied to ceiling fans as the latter promote mixing and influence room air temperatures.

Both $doES$ and $doSS$ can be used to quantify ES and SS in any type of building where preserving certain temperatures is a requirement for thermal comfort and occupant wellbeing (residential, non-residential, commercial buildings).

For this study, $degree.hours$ (K.h) was used as the resilience key performance indicator [53]. It accounts for the occupied hours during which the zone temperature exceeds a pre-defined threshold by 1 K [54]. For this study 24°C was chosen as the overheating threshold

for European buildings according to the CIBSE TM52 standard [55]. $degree.hours$ is calculated as follows:

$$degree.hours = \int_1^2 [T(t) - T_{threshold}]_+ \, dt \qquad (6)$$

where T is the indoor air temperature (°C); $T_{threshold}$ is the 24°C temperature threshold [°C]; t is time (h). The acceptable threshold according to the same standard is equal to 6 K.h.

To compare different shocks having different durations (especially **ES**), Method A as described in Annex F of the EN 16798 [56] was selected. Following this method, the percentage of occupied hours when the zone operative temperature is above 24°C was evaluated. A percentage of occupied hours below 5% is considered as **acceptable** and below 3% is considered **good**.

3. Methods

Figure 2 illustrates the methodology flowchart which illustrates the steps followed throughout this study. The first step was to model in Modelica, the case study building equipped with the different passive cooling strategies. The case study building, its technical installations and their control were described in section 3.1. Step 2 consisted of the validating the model experimentally in one of the case study rooms for a base case of no shock and a shock case. This step is important to make sure the model's temperature predictions were reliable to conduct the next step of this study which is the parametric analysis (Step 3). The analysis was conducted for different *doES* and *doSS* and combinations of the latter. Finally, the resilience performance of the different cooling strategies were discussed in Step 4, as well as comparisons of different shock types, and assessment of the impact of thermal mass to explain some of the discrepancies between the two TLRs.

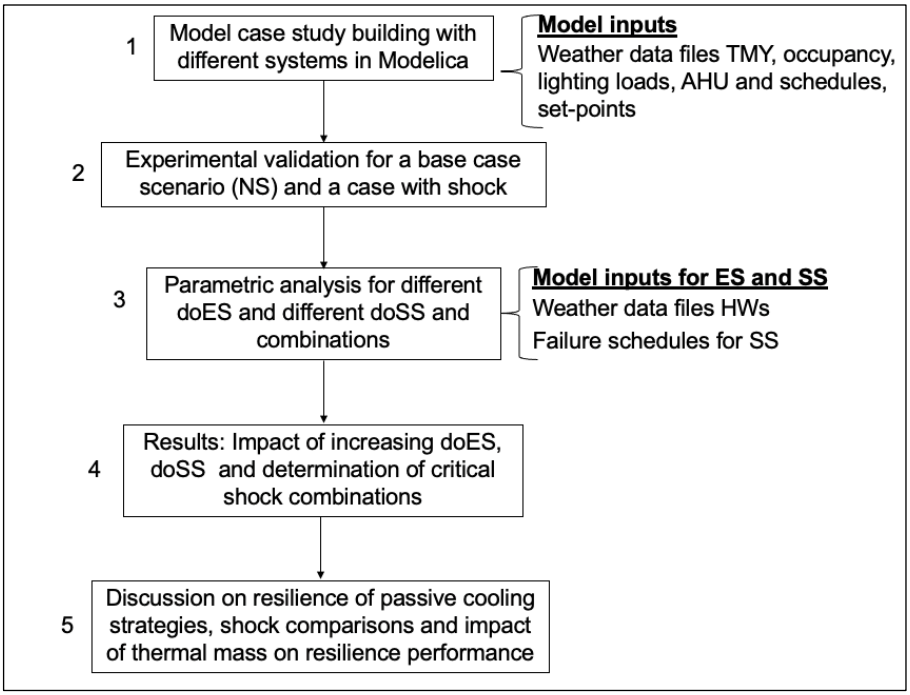

Fig. 2. Methodology flowchart

3.1. Building and Systems' description

The case study building is a real-use educational building, situated at the Ghent Campus, KU Leuven, Belgium. The building consists of two lecture rooms, **E120** (1st floor) and **E220** (2nd floor) (13.28 m length × 10.69 m width × 2.7 m height) that can each seat a maximum of 80 students. The Menerga AHU [57] serving the lecture rooms resides in a technical room on the top floor. **Figure 3** illustrates a schematic of the building and its AHU. The building was designed according to Passive House Standard [58]. The two test lecture rooms (TLRs) are identical zones with different air tightness. The airtightness n_{50} of **E120** and **E220** is 0.41 h^{-1} and 0.29 h^{-1} respectively. **E120** has a brick external wall with exterior insulation and **E220** has light-weight timber frame external wall. Both exterior walls have the same U-values of 0.15 $W/m^2.K$. Both lecture rooms have concrete slab floor with cellulose insulation and have U-values of 0.15 $W/m^2.K$. The roof is wooden frame with cellulose insulation and have U-value of 0.14 $W/m^2.K$ [59]. The composition of the envelope was presented in **Table S1** in the **SI**.

Each lecture room has ten triple glazed windows (U-value = 0.65 $W/m^2.K$, window-to-wall ratio = 26.5%, window-to-floor ratio = 13%): six on the southwest facade and four on the

northeast façade (**Fig. 3**). All windows have manually operable external screens. The screens on the southwest façade were additionally automated (shading ON for 15 minutes when the global solar radiation on the windows is above 250 W/m^2).

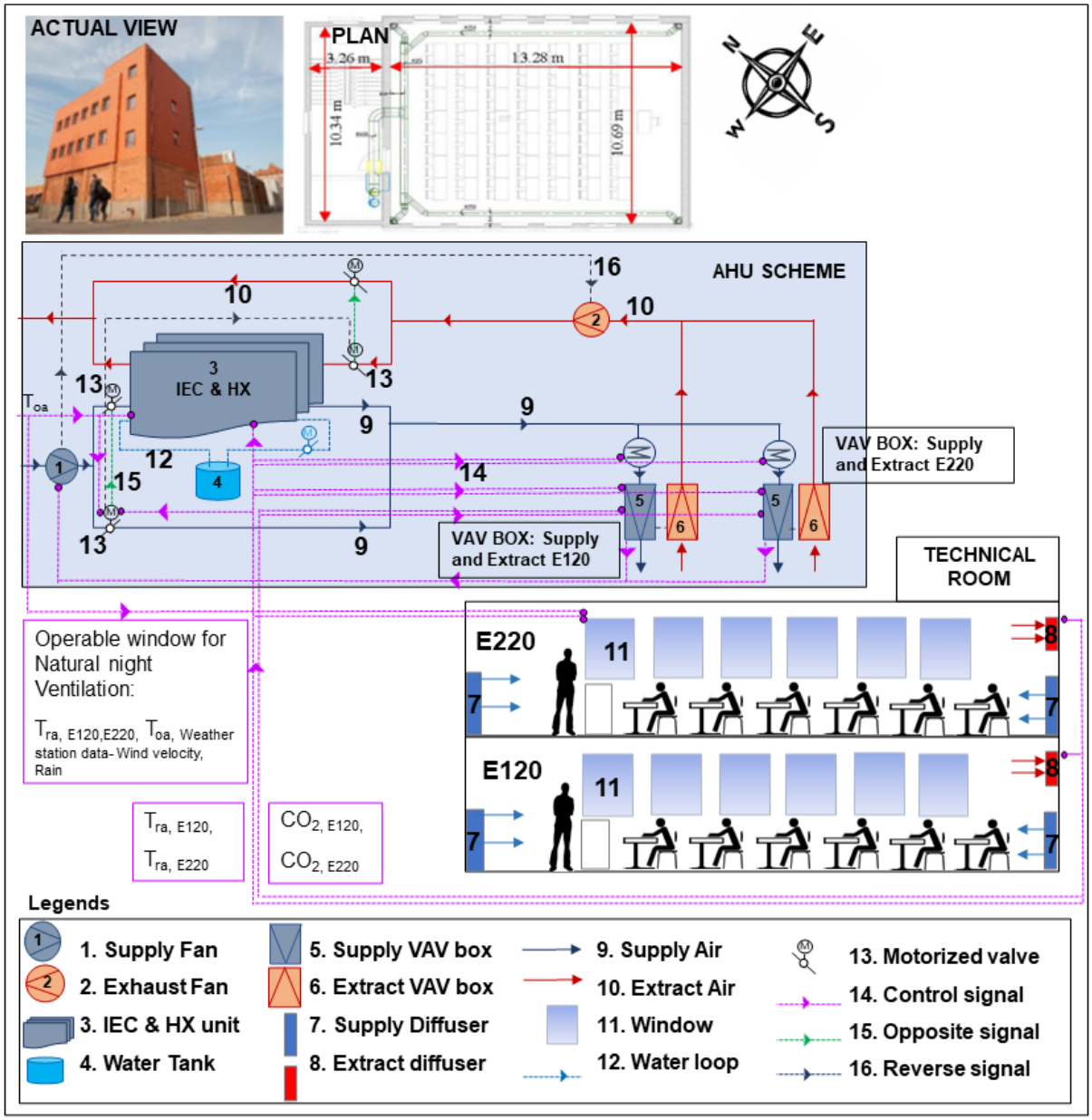

Fig. 3. Schematic of the test lecture building consisting of **E120**, **E220** and the AHU

The AHU operates from Monday to Friday from 7:30 a.m. to 6:00 p.m. and is shut off during the weekends as there are no classes. The building is equipped with an all-air system with balanced mechanical ventilation. The air is supplied via a displacement ventilation system in both lecture rooms (**Fig. 3**). The supply and extract fans supply a minimum airflow of 400

m^3/h and a maximum of 4400 m^3/h. Four variable air volume (VAV) boxes regulated by Proportional Integral (PI) signals control the airflow of the demand-controlled ventilation (DCV) system based on competing CO_2 and temperature demands [60]. The PI control compares the level of deviation of each room temperature from its 22°C setpoint and the level of deviation of each room's CO_2 concentration from an assigned threshold of 1000 ppm [61].

During the cooling season in the daytime, the lecture rooms are passively cooled by an **IEC** from 7:30 a.m. until 6:00 p.m., having a maximum capacity of 13.1 kW. It is composed of wet channels equipped with cooling pads wetted with water originating from a feeder tank. A secondary flow of air – in this case the exhaust air from the lecture rooms, flows through the cooling pads. The clean outdoor air also enters the AHU through a supply fan. If the **IEC** operation is triggered, all the supply flow is completely diverted through the **IEC** and the flow is maximum. The **IEC** operation is regulated via a control block consisting of two types of controls: an ON/OFF controller and a hysteresis controller. The control block takes as input measurements of the lecture rooms' room air temperatures ($T_{ra,E120}, T_{ra,E220}$) and the outdoor dry bulb temperature T_{oa}. The **IEC** is triggered if one of the following conditions is true:

a) ON/OFF controller detects that $T_{oa} \geq 22$°C or

b) Hysteresis controller detects that max($T_{ra,E120}, T_{ra,E220}$) ≥ 24.5°C.

Once triggered, the hysteresis controller will keep the **IEC** in operation until max ($T_{ra,E120}, T_{ra,E220}$) ≤22.5°C.

The supply VAV boxes controls the flow rate for each lecture depending on the demand and cooled air is supplied to **E120** and **E220**.

The building is also equipped with **NNV** for pre-cooling of the lecture rooms during night-time [62]. **NNV** is activated from 10:00 p.m. to 6:00 a.m. from 1st April to 31st October, by opening of 10 motorized windows on both southwest and northeast façades [62]. The total

effective operable area of these windows is 4% of the floor area. Once open, the window will remain open for at least 15 minutes if all of the following conditions are met simultaneously:

a) Max ($T_{ra,E120}$ *or* $T_{ra,E220}$) ≥ 22°C and ≥ than the outdoor air temperature T_{oa} by 2°C

b) Maximum zone temperature ($T_{ra,E120}, T_{ra,E220}$) of the previous day ≥ 23°C

c) T_{oa} >12°C

d) RH < 70%

e) There is no rainfall and the wind velocity < 10 m/s measured at a height of 10 m from ground level.

3.2. Modelica model and inputs

A simulation model of the building was developed using Modelica [46] in the Dymola environment (2020x) [63] and using the "Integrated District Energy Assessment by Simulation" (IDEAS) [64] library (Version v2.2.1). Modelica is an open-source, equation-based modelling language with embedded libraries like IDEAS containing validated sub-models that can accurately represent the building dynamics, HVAC systems, the control strategies as well as varying events with different time scales. **Figure 4** illustrates the Modelica model of the building as seen in Dymola. Each lecture room was modelled as a separate thermal zone by the zone component (2) and the envelope components (outer walls (19), windows (20, 22), partitions (21)). The zone model was considered to achieve well-mixed and homogeneous conditions of temperature. The floor of **E120** and walls connecting the TLRs to the staircase were modelled as adiabatic. The building has multiple systems (4, 5, 6, 7, 8, 9, 22) with control blocks, that regulate their operation during heating/cooling seasons to maintain constant comfortable temperatures (11, 12, 16, 23). Additionally, for DCV, there is a competing temperature vs. CO_2 demand that is continuously monitored (13, 14, 15). Description of the different model components can be found in the **SI**.

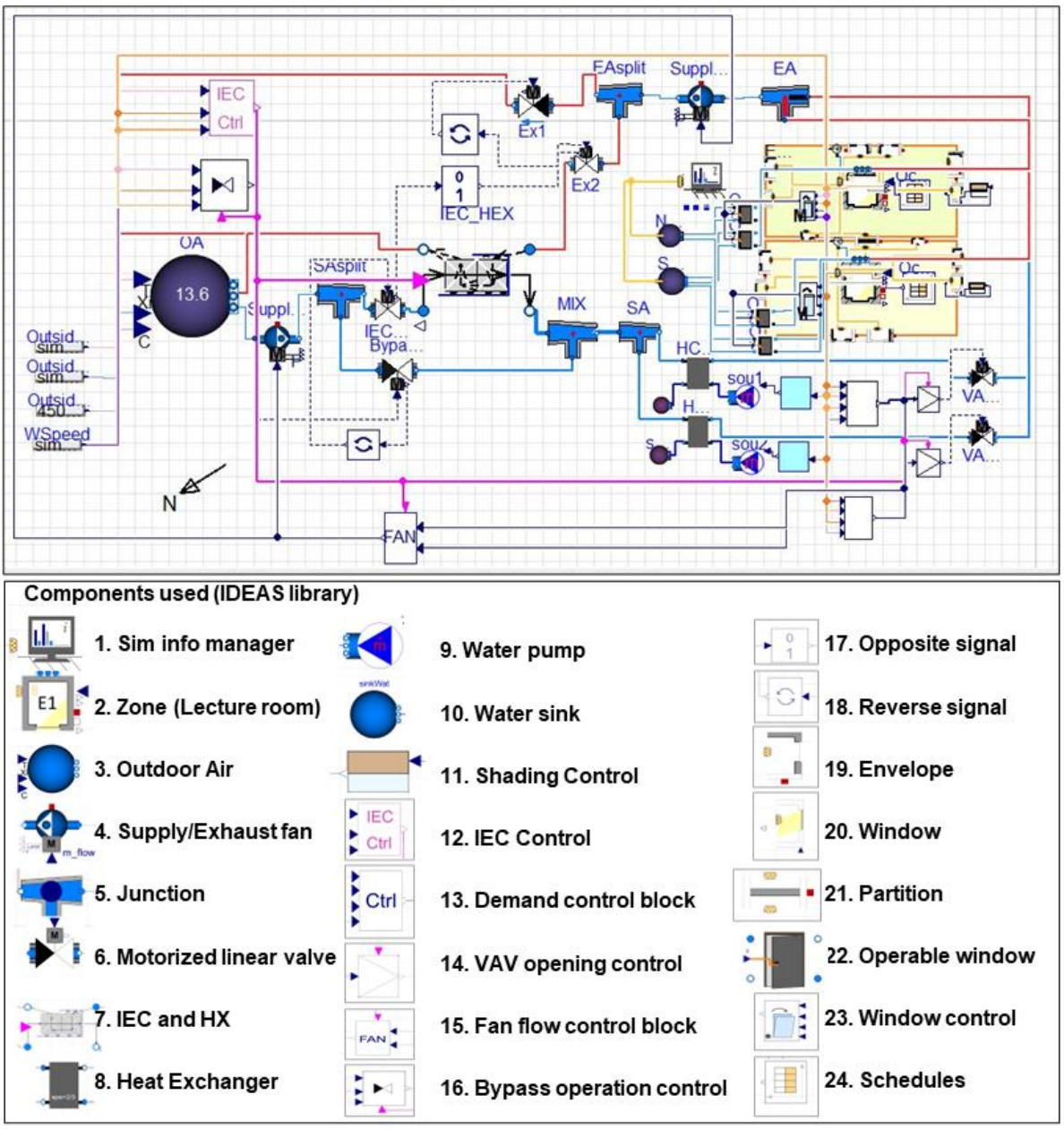

Fig. 4. Modelica Model of the test lecture room building consisting of the building envelope, and systems + controls

The model inputs were the weather data in the Sim Info Manager component (1) and the occupancy schedules (24). The sensible and latent heat generation from occupants were 75 W and 45 W respectively during sedentary activities [65]. The occupancy schedule of the two lecture rooms was taken as input from the building monitoring system (BMS). Occupancy in the lecture rooms was tracked by an Acurity 3D vertical optical counting system installed in the lecture rooms 1 m from the door entrance [66]. The two TLRs, were typically used from

Monday to Friday, between 8:15 a.m. and 6:00 p.m. following the class schedule in **Table S2**. **Figure 5** represents the weekly occupancy schedule from 8th to 15th of June 2021. This week was chosen for the simulations since the full classes schedules were conducted each day of the week for each TLR (**Table SI 2**). Since the effect of the simulated shocks will be monitored for several weeks during and after the shock, this occupancy schedule was repeated periodically. Sensible heat generation due to lights was defined in Modelica as 700 W in each zone model. The lights only turned on when occupants were present.

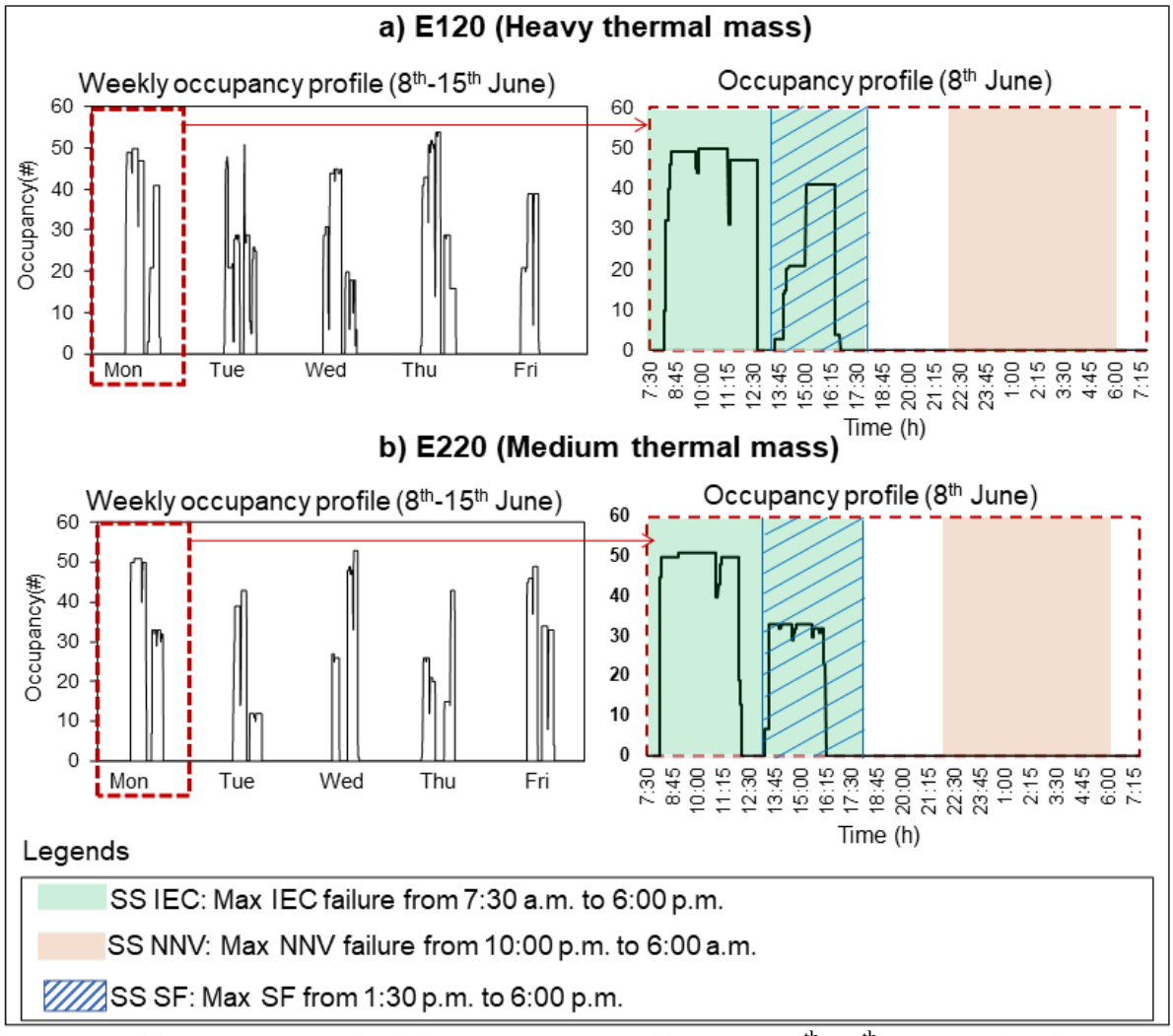

Fig. 5. Weekly occupancy schedules in: a) **E120** and b) **E220** (8th-15th June) and a close up of the occupancy schedule on the 8th of June when **SS** was inflicted

Simulations were run with 1 minute time step to capture the temporal variation of the AHU**, IEC**, **NNV** and shading operations and temperatures. The simulations were run from 1

week prior to stabilize the solution on the period of shock, and fifteen days after to check the extend of shock impact on thermal conditions of the TLRs. Each simulation period varies according to the duration of each shock type.

3.3. Experimental model validation

Figure 6 illustrates the experimental setup in **E120.** The experimental method of Al Assaad et al. [63,64], employing heated cylindrical thermal manikins, was used to validate the numerical predictions of the Modelica model ($T_{ra,E120}$, operation of **IEC** and **NNV**). Thermal manikins were used instead of occupants in the experiment to provide controlled input for internal gains in the experimental set up as well as the simulation model. The actual occupancy schedules were later on used for the parametric study. 21 manikins were uniformly distributed across **E120** to reduce spatial gradients in temperature distribution [65]. Temperatures were monitored at the room exhaust diffuser at 1-minute intervals using VAISALA GMW90 sensors [69] that measure temperatures between -5°C and 55°C with an accuracy of ±0.5°C. Apart from these measurements, continuous logging of the parameters like supply and return air temperatures, operation signal of the AHU, **IEC**, **NNV**, VAVs etc., was done using the BMS [70]. The Modelica model was validated under normal operating conditions without shocks (**NS**=base case) and a shock case (30-minute power outage) [68]. Two experimental scenarios were conducted during the 2nd week of August 2021 and lasted one day each. No classes were scheduled during that period. The base case was conducted on the 8th of August. The second case is a shock scenario of 30 min power outage (PO) shock and was conducted on the 14th August 2021. The PO was manually inflicted by turning off the AHU for 30 minutes starting 3:00 p.m. In both cases, the manikins' heat sources were turned on 12:00 p.m. and turned off at 5:00 p.m. This type of shock is a combination of two **SS** (failure of **IEC**, and ventilation failure-**VF**). It was chosen due to its severe impact, ease of implementation and since triggering an **ES**

is not possible in a real case study. More details on the experimental methodology and protocol can be found in the **SI.**

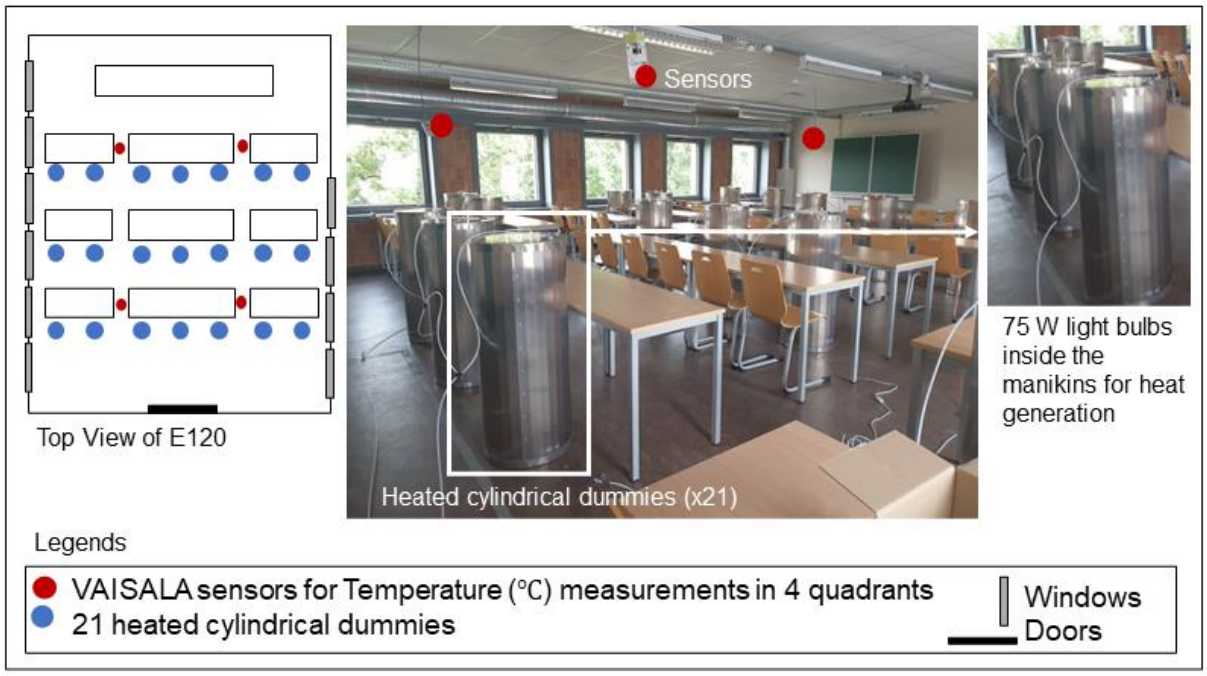

Fig. 6. Experimental setup in **E120** with 21 heated cylinders and measuring equipment.

Figure 7 shows a comparison of predicted vs. measured $T_{ra\,E120}$, operation of **IEC** and **NNV** during - (a) base case and (b) 30 min power outage. For normal operation (**Fig. 6(a)**), $T_{ra\,E120}$ increased from 22.3±0.5°C at 8:15 a.m. up to 22.3±0.5°C at 12:30 p.m. due to increase in occupants and reached a maximum of 24.4±0.5°C at 3:30 p.m. due to heat build-up (internal gains due to occupants, equipment and solar gains). Experimentally, the **IEC** was triggered at 11:07 a.m., due to outdoor conditions. **IEC** is deactivated at 6:00 p.m. After the manikins were turned off at 5:00 p.m., $T_{ra\,E120}$ decreased gradually to reach 22.5±0.5°C at 9:00 p.m.. **NNV** operation started at 10:00 p.m. $T_{ra\,E120}$ decreased by 1.3°C. **NNV** was inactive for 30' from 2:00 a.m. to 2:30 a.m. as $T_{ra\,E120}$ reached below 21.5°C. The same temperature trend and operation of **IEC** and **NNV** can also be observed in the simulation model. There are two conditions that the results of the simulation model must meet to be considered validated-(a) The MAE (Mean absolute value of error) < 1°C and (b) RMSE (Root mean squared error) <1.5°C [71]. The MEA and RMSE between the simulated model and the monitored $T_{ra\,E120}$ is 0.75°C

and 0.95℃. Good agreement was obtained between predicted and measured values of $T_{ra\,E120}$ (maximum relative error of 4.6%). During 30' power outage (**Fig. 7(b)**), 21 manikins were activated at 1:00 p.m. **IEC** was activated in experimental setup at 10:50 a.m. as T_{oa} reached 22°C. Due to **IEC** activation, $T_{ra\,E120}$ dropped by ±0.5°C at 11:00 a.m.. After the manikins were activated at 1:00 p.m., $T_{ra\,E120}$ increased from 22.7±0.5°C to reach 24.4±0.5°C at 3:00 p.m. A power outage (AHU shut-down) was inflicted from 3:00 p.m. to 3:30 p.m. **IEC** operation was restored at 3:30 p.m., but $T_{ra\,E120}$ increased to 26.0±0.5°C at 5:00 p.m. due to insufficient **IEC** operation and high wet bulb temperature. The manikins were turned off at 5:00 p.m. **NNV** was activated at 10:00 p.m. and $T_{ra\,E120}$ dropped by 0.5°C. The same temperature trend and operation of IEC and NNV can also be observed in the simulation model. MEA and RMSE between the simulated model and the monitored $T_{ra\,E120}$ is 0.95℃ and 1.10℃ respectively. Good agreement was obtained between predicted and measured values of $T_{ra\,E120}$ and the measured vs simulated IEC and NNV operation times (maximum relative error of 1.2%).

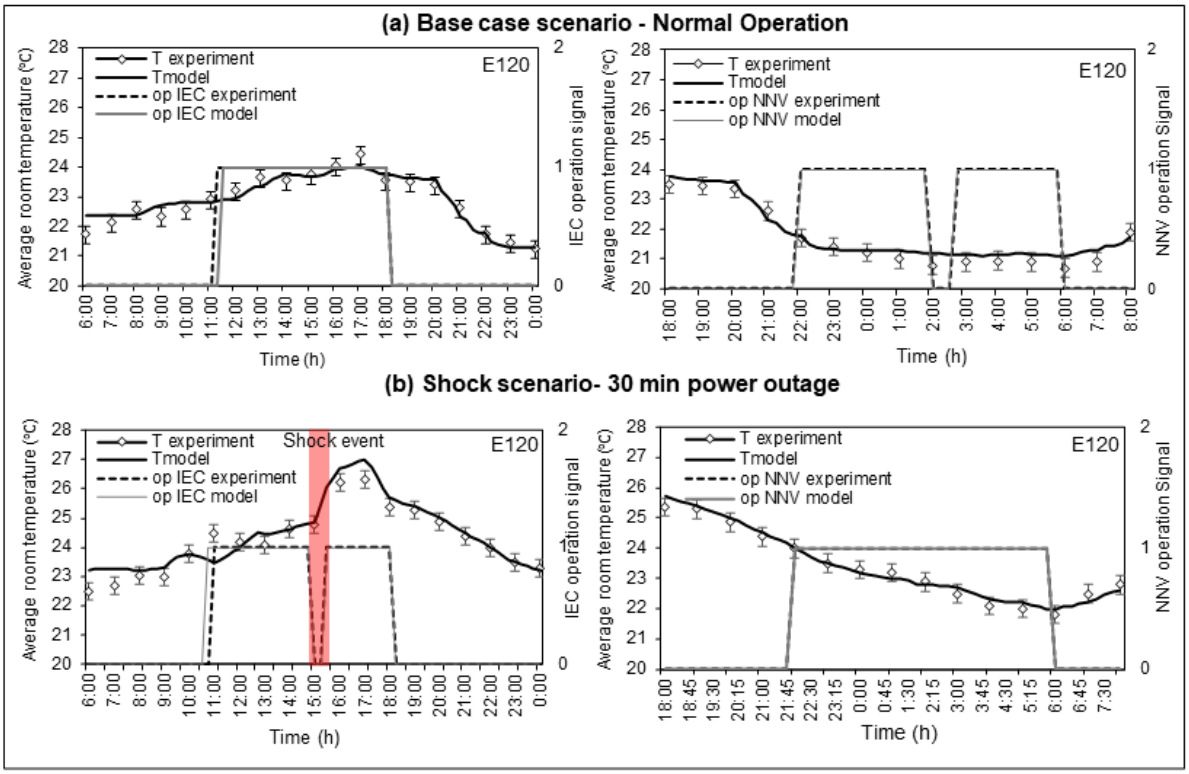

Fig. 7. Comparison of the predicted and measured temperatures of **E120**, operation of **IEC** and **NNV** for: (a) normal operation and (b) 30 minute power outage

3.4. Parametric study

A parametric study was conducted using the validated building model to assess and compare the impact of ES, SS and combinations of them. For benchmarking, base case scenarios with no shock (**NS**) were defined for each shock type.

3.4.1. Selection of ES

HWs were selected to investigate the impact of **ES** on the thermal environment. Ouzeau et al. [72] characterized **HW**s by their **intensity** (i.e., maximum daily mean temperature °C reached during the heatwave), **duration** (days) and **severity** (i.e., °C.days over a threshold). To be classified as a **HW**, the dry bulb temperature should simultaneously exceed a threshold temperature and a certain duration. These thresholds are determined for each country based on the methodology of Ouzeau et al. [72]. In Belgium, if the temperatures exceed 25℃ for a minimum of 5 days and if among these 5 days, temperatures exceed 30℃ for a minimum of 3 days, then the event can be considered as a **HW**. For Belgium, a heatwave ends if temperatures drop below 20.2°C or if temperatures go below 21.8°C for 3 consecutive days.

Corresponding **HW** and **TMY** (reference case, equation (2)), weather data files are needed as input to the Modelica model. Using the methodology developed by the IEA EBC Annex 80 [73] and Machard et al. [74], **1 TMY** and **multiple HW** weather data files were extracted for three time periods: **Contemporary** (2001-2020), **mid-term** (2041-2060) and **long-term** (2081-2100). The contemporary **TMY** (2010s) file was selected as it can properly demonstrate the most typical pattern of performance during recent summers. In each period, the most extreme **HW** were chosen (i.e., the most intense, the most severe, and the longest). **Table 1** illustrates the selected **HW** and their characteristics. **Figure 8** illustrates the temporal variation of outdoor dry bulb temperature during each **HW** and the corresponding **TMY** period.

More information on the weather data generation method and the **HW** selection process can be found in **SI**.

Table 1. Selected **HW**s for Gent

Period	**ID**	**Characteristics of HWs**[1]			
		Intensity	**Duration** (days)	**Severity** (°C.days)	$doES_{HW}$[2]
Contemporary	1A	30.0 °C	10 (June 24 - July 3)	18	0.167
	1B	31.1 °C	27 (July 5 - July 31)	26.3	0.205
Mid-term	2A	28.6 °C	6 (June 29 - July 4)	7.2	0.060
	2B	30.9 °C	16 (June 27 - July 12)	25.5	0.179
Long-term	3A	30.1°C	34 (July 8 - Aug 10)	36.8	0.311
	3B	33.3°C	45 (July 2 - Aug 15)	46.1	0.368

[1] *Corresponding TMY weather data files (reference case) have the same duration and occurrence period as HWs*
[2] $\overline{T_{oa,ES}}$ *in equation 2 corresponds to* $\overline{T_{oa,HW}}$. t_{shock} *(days) is the duration of the HW being evaluated, whereas* $t_{shock,max}$ *(days) is the longest predicted heatwave in the span of the next 100 years (45 days)*

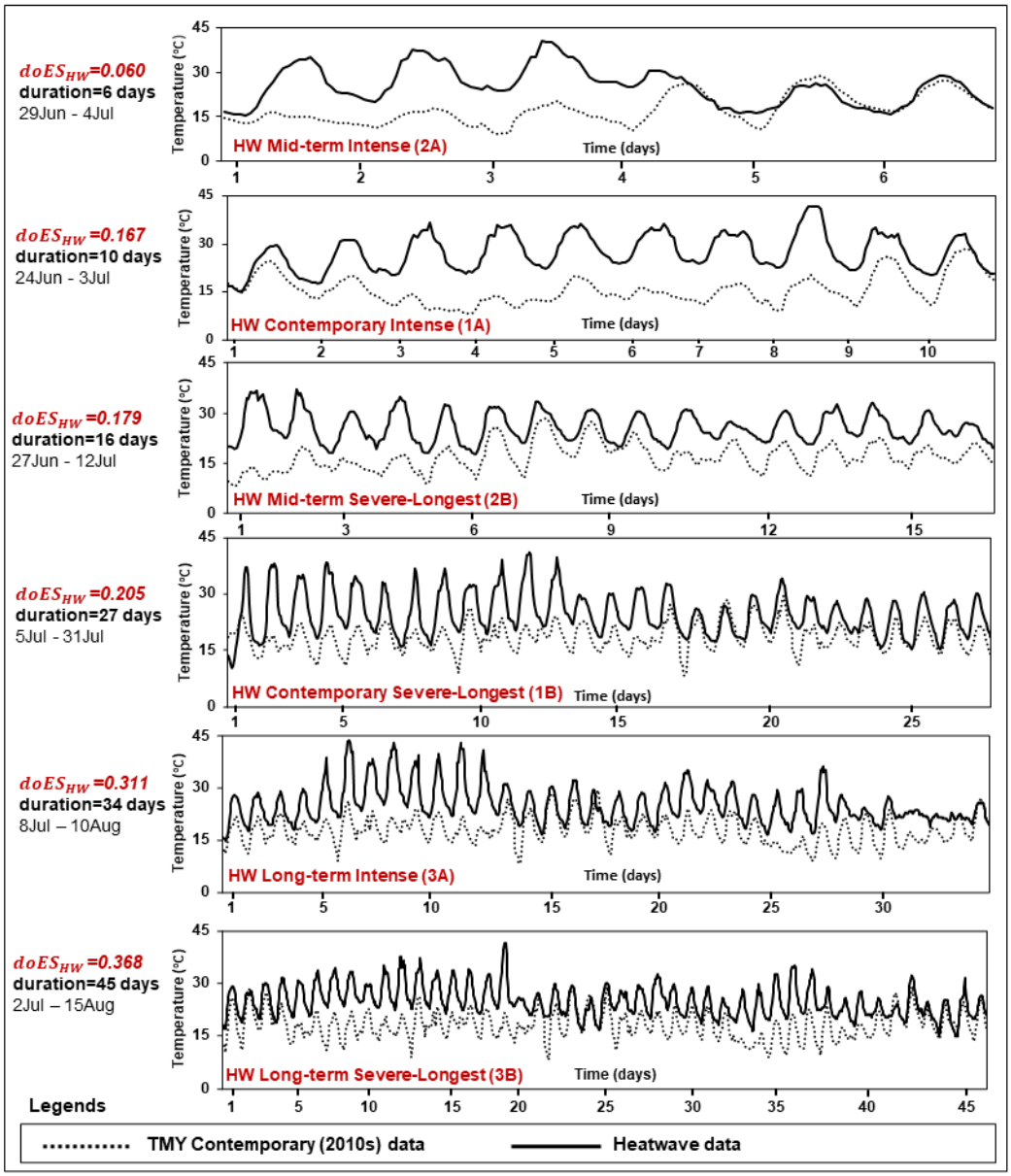

Fig. 8. Outdoor dry bulb temperature variation, of selected **HW**s and **TMY**

3.4.2. Selection of SS

To evaluate the impact of increasing degree of **SS, SF (**$doSS_{SF}$), **IEC failure** ($doSS_{IEC}$) and **NNV failure** ($doSS_{NNV}$) were inflicted upon the two TLRs in the beginning of the week (Monday -June 8th). For each of the **SS**, the benchmark case is a base case with **NS** having the same duration as each shock case. **Table 2** presents the different **SS** simulation scenarios. For each **SS**, the shock was increased from 30' to its maximum operation duration with an increment of 30' (maximum operation time is 630' for **IEC**, 270' for **SF** and 480' for **NNV**). For **IEC**, the shock started at 7:30 a.m. as it is the starting time of the AHU. For **SF**, the shock started at 1:30 p.m. since solar radiation increases on the southwest façade starting from 1:30 p.m. The shading operating schedule from the BMS also demonstrated activation of shading during summer from 1:30 p.m. onwards. For **NNV** failure, the shock started at 10:00 p.m. (i.e., start time of NNV operation). . $\overline{T_{sa,IEC}}$, $\overline{T_{sa,NS}}$, $\overline{T_{wn,SF}}$, $\overline{T_{wn,NS}}$, $\overline{T_{ra,NNV}}$ and $\overline{T_{ra,NS}}$ are outputs from the validated Modelica model.

To assess the most critical time of SS occurrence, each SS was inflicted at different times during system operation. IEC failure can occur during any time period between (7:30 a.m. to 6:00 p.m.), the time of shock occurrence can have different effects depending on the occupancy and thermal storage. SF can occur during any time period between (1:30 p.m. to 6:00 p.m.) and the time of shock occurrence can have different effects depending on the solar radiation on the glazing. NNV failure can occur during any time between (10:00 p.m. to 6:00 a.m.) and the time of shock occurrence can have different effects depending on the difference due to outdoor and indoor conditions (temperature, RH (%), wind speed and direction) and also on the thermal storage of the two lecture rooms. Table 2 illustrates the different times of occurrence of each type of SS.

Table 2. Parametric study table for **SS**

Type of shock	Maximum shock duration	Time of occurrence	Calculated *doS*	Justification
NS	-	-	-	No shock occurs (base case)
SS: SF: Failure of automated shading				
Automated **SF** $[doSS_{SF}]$[1]	270 min	1:30 p.m.	[0.006 - 0.323] for **both TLRs**	0.006 corresponds to 30' of **SF** starting from 1:30 p.m. and 0.323 corresponds to max $doSS_{SF}$ of 270 minutes: 1:30 p.m. - 6:00 p.m.
	180 min	3:00 p.m.	[0.002 - 0.323] for **both TLRs**	
SS - VF: Failure of IEC				
CSF: IEC failure $[doSS_{IEC}]$[2]	630 min	7:30 a.m.	[0.015 - 0.127] for **both TLRs**	0.015 corresponds to 30' of **IEC failure** starting from 7:30 a.m. and 0.127 corresponds to max $doSS_{IEC}$ of 630': 7:30 a.m. - 6:00 p.m. $doSS_{IEC}$ range varies in the two TLRs due to different occupancy level and the demand for the supply air.
	495 min	9:45 a.m.	[0.004 - 0.127] for **E120** [0.005 – 0.127] for **E220**	
	180 min	3:00 p.m.	[0.005 - 0.127] for **E120** [0.011 – 0.127] for **E220**	
SS - VF: Failure of NNV				
VF: NNV failure $[doSS_{NNV}]$[3]	480 min	10:00 p.m.	[0.001 - 0.047] for **E120** [0.001 -0.021] for **E220**	0.001 corresponds to 30'of **NNV failure** starting from 10:00 p.m.. 0.047 and 0.021 are max $doSS_{NNV}$ for 480': 10:00 p.m.- 6:00 a.m. for **E120** and **E220** respectively. $doSS_{NNV}$ range varies in the two TLRs due to different heat gains during the day (occupancy) and difference in air-tightness for both the TLRs
	360 min	12:00 a.m.	[0.0009 - 0.047] for **E120** [0.0008 - 0.021] for **E220**	
	240 min	2:00 a.m.	[0.00075- 0.047] for **E120** [0.0006 - 0.021] for **E220**	
	120 min	4:00 a.m.	[0.0005 - 0.047] for **E120** [0.0003 - 0.021] for **E220**	

[1] $\Delta(doSS_{SF}) = 0.006$ *equivalent to 30' increment of* ***SF***
[2] $\Delta(doSS_{IEC}) = 0.015$ *equivalent to 30' of* ***IEC failure***
[3] $\Delta(doSS_{NNV}) = 0.001$ *equivalent to 30' of* ***NNV failure***

3.4.3. Shock combinations

Shock combinations were assessed to quantify how critical a shock is if it is accompanied by another shock (e.g., power outages being common during heatwaves). For the shock combination of **ES**+**SS** scenario, the mid-term (2050s) **HW** (**ID = 2A;** $doES_{HW}$ = 0.06, **Table**

1) was selected. This **HW** was selected since it is in line with the past and recent HWs in Belgium in terms of daily average outdoor air temperature and in duration (i.e., most relevant for current times and buildings). The HW (ID = 3B, $doES_{HW} = 0.368$), with highest impact on the two TLRs was not selected since it was predicted to occur in the long-term future scenario (2081-2100) when the current building stocks are assumed to have undergone improvement in construction techniques, energy efficient cooling strategies and other overheating mitigation strategies.

SS was inflicted on the hottest day of the **HW** (in this case-1st July). For a **SS + SS combination,** the maximum shock duration for each SS was inflicted. **Table 3** gives an overview of the different chock combinations simulation scenarios.

Table 3. Parametric study table for **Shock combinations**

Type of shock 1	**Type of shock 2**	**Maximum shock duration**	**Calculated doS for both TLRs**	**Time of occurrence**
NS	NS	-	0.00	-
ES and SS combinations[1]				
HW	IEC	HW= 6 days IEC= 630’	$doES_{HW}$ = 0.060 $doSS_{IEC}$ = 0.127	IEC : 7:30 a.m.
HW	SF	HW= 6 days SF= 270’	$doES_{HW}$ = 0.060 $doSS_{SF}$ = 0.323	SF : 1:30 p.m.
HW	NNV*****	HW= 6 days NNV= 480’	$doES_{HW}$ = 0.060 $doSS_{NNV}$ = 0.050	NNV : 10:00 p.m.
HW	IEC and VF (AHU failure)	HW= 6 days IEC = 630’ VF= 630’	$doES_{HW}$ = 0.060 $doSS_{VF}$ = 0.168 $doSS_{IEC}$ = 0.127	Ventilation system and IEC failure : 7:30 a.m.
HW	IEC and SF	HW= 6 days IEC = 630’ SF= 270’	$doES_{HW}$ = 0.060 $doSS_{IEC}$ = 0.127 $doSS_{SF}$ = 0.323	IEC : 7:30 a.m. SF : 1:30 p.m.
HW	IEC and NNV*	HW= 6 days IEC = 630’ NNV= 480’	$doES_{HW}$ = 0.060 $doSS_{IEC}$ = 0.127 $doSS_{NNV}$ = 0.05	IEC : 7:30 a.m. NNV : 10:00 p.m.
HW	SF and NNV*	HW= 6 days SF=270’ NNV= 480’	$doES_{HW}$ = 0.060 $doSS_{SF}$ = 0.323 $doSS_{NNV}$ = 0.050	SF : 1:30 p.m. NNV : 10:00 p.m.
HW	IEC, SF and NNV*	HW= 6 days IEC = 630’ SF= 270’ NNV= 480’	$doES_{HW}$ = 0.060 $doSS_{SF}$ = 0.323 $doSS_{IEC}$ = 0.127 $doSS_{NNV}$ = 0.050	IEC : 7:30 a.m. SF : 1:30 p.m. NNV : 10:00 p.m.

HW	VF, IEC and NNV* (AHU and NNV* failure)	HW= 6 days VF= 630' IEC = 630' NNV= 480'	$doES_{HW}$= 0.060 $doSS_{VF}$ = 0.168 $doSS_{IEC}$ = 0.127 $doSS_{SF}$ = 0.323	Ventilation system and IEC failure : 7:30 a.m. SF : 1:30 p.m. : 10:00 p.m.
HW	VF, IEC, SF and NNV* (Power outage)	HW= 6 days VF= 630' IEC = 630' SF= 270' NNV= 480'	$doES_{HW}$= 0.060 $doSS_{VF}$ = 0.168 $doSS_{IEC}$ = 0.127 $doSS_{SF}$ = 0.323 $doSS_{NNV}$ = 0.05	Ventilation system and IEC failure:7:30 a.m. SF : 1:30 p.m. NNV : 10:00 p.m.
SS and SS combinations[2]				
IEC	VF	VF= 630' IEC = 630'	$doSS_{VF}$ = 0.168	Ventilation system and IEC : 7:30 a.m.
IEC	SF	IEC = 630' SF= 270'	$doSS_{SF}$ = 0.323	IEC : 7:30 a.m. SF : 1:30 p.m.
IEC	NNV*	IEC = 630' NNV= 480'	$doSS_{NNV}$ = 0.050	IEC : 7:30 a.m. NNV : 10:00 p.m.
SF	NNV*	SF= 270' NNV= 480'	$doSS_{NNV}$ = 0.050	SF : 1:30 p.m. NNV : 10:00 p.m.
IEC	SF and NNV*	IEC = 630' SF= 270' NNV= 480'	$doSS_{SF}$ = 0.323 $doSS_{NNV}$ = 0.050	IEC : 7:30 a.m. SF : 1:30 p.m. NNV : 10:00 p.m.
VF	IEC and SF	VF= 630' IEC = 630' SF= 270'	$doSS_{VF}$ = 0.168 $doSS_{SF}$ = 0.323	Ventilation system and IEC failure : 7:30 a.m. SF : 1:30 p.m.
VF	IEC, SF and NNV* (Power outage)	VF= 630' IEC = 630' SF= 270' NNV= 480'	$doSS_{VF}$ = 0.168 $doSS_{SF}$ = 0.323 $doSS_{NNV}$ = 0.050	Ventilation system and IEC failure : 7:30 a.m. SF failure :1:30 p.m. NNV:10:00 p.m.

[1] SS (one or more types) occur on the hottest day of the 6 day long HW period.
[2] One or more system shocks occur on the beginning of a week in summer period (Monday 8th June)
** Common value of $doSS_{NNV}$*

4. Results

Section 4.1 presents the base case scenario for **SS** and for **ES**. Section 4.2 presents the impact of increasing degree of shock for **ES** and **SS**. Section 4.3 reports the impact of different shock combinations.

4.1. Base case scenario (NS)

Figure 9 illustrates the temporal evolution of T_{ra} for both TLRs, occupancy, **IEC** and **NNV** operation of the base case scenario during a normal operation with **NS** (doS = 0.00) on 8th June. $\overline{T_{oa\,TMY}}$ on 8th June was 19.2°C with a maximum of 21.6 °C at 3:00 p.m.

The temporal trend of T_{ra} in both TLRs was proportional to their respective occupancy schedules, T_{oa} and the solar gains. During occupancy period (8:15 a.m. to 4:30 p.m.), $\overline{T_{ra\,E120}}$ and $\overline{T_{ra\,E220}}$ were 23.8℃ and 24.3℃ respectively and $T_{ra,\max\ E120}$ of 24.5℃ was reached at 4:25 p.m. while $T_{ra,\max\ E220}$ of 24.8℃ at 4:10 p.m. At 8:15 a.m., T_{ra} started to increase by 1.5℃ in both TLRs due to gradual increase in occupancy (46 students for **E120** and 48 students for **E220**). The **IEC** was triggered at 10:50 a.m. as $T_{ra,220}$ reached 24.5℃. However, T_{ra} kept increasing due to internal loads despite **IEC** operation and reached 24.7℃ at 12:30 p.m. During the break at 12:30 p.m., there was a drop of 0.3℃ in both TLRs due to the sudden decrease of occupants. **IEC** was unable to lower the temperature to the setpoint due to high occupancy, solar gains especially on the SW façade and high *RH*. After 6:00 p.m., T_{ra} in both TLRs kept increasing until 10:00 p.m. due to thermal storage effect of the envelope. Once **NNV** was active, T_{ra} for both **E120** and **E220** decreased below 24.0℃ within 30'. $\overline{T_{ra\,E120}}$ and $\overline{T_{ra\,E220}}$ during night (10:00 p.m. to 6:00 a.m.) were 22.4℃ and 24.0℃ respectively. Daytime and night-time $T_{ra,\max}$ of **E220** was higher than **E120** by 0.7℃ and 2.0℃ respectively. $degree.hours$ were 0.64 and 3.84 for **E120** and **E220** respectively (< 6, acceptable, no overheating).

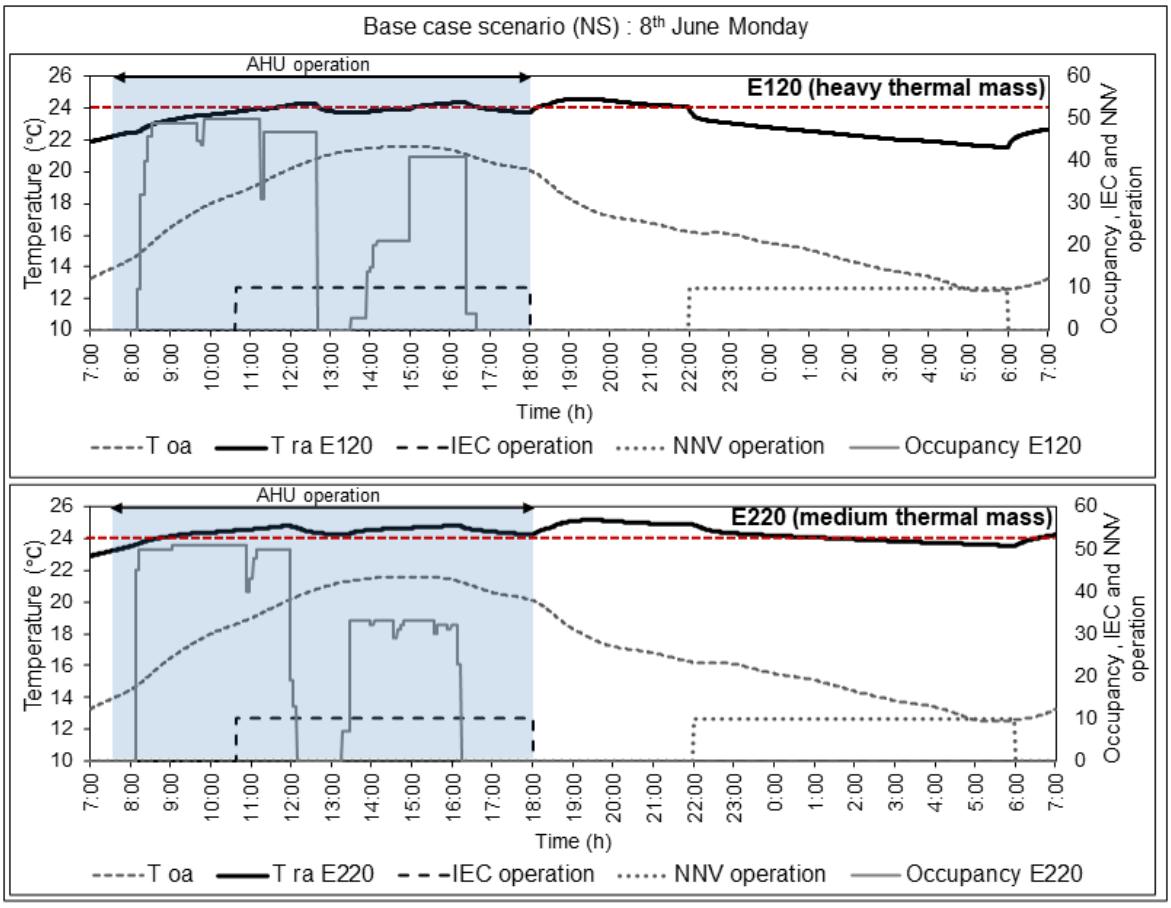

Fig. 9. Temporal evolution of T_{oa}, T_{ra} for **E120** and **E220**, occupancy of both TLRs and operation of **IEC** and **NNV** on June 8th for case of **NS**

Figure 10 illustrates the (0.4% and 2.8%) of occupied hours above a 24°C threshold for **E120** and **E220** respectively base case NS scenarios, used to compare the impact of the 6 extreme **HW**s (**Table 1)**. Each **HW** will be assessed for the same duration as TMY (2010s). As $T_{oa\,TMY}$ gets warmer in July and August compared to June, $degree.hours$ for each TLR increased. Temporal variations of room air temperatures in **E120** and **E220** can be found in **SI**. In all 6 base case scenarios, (%) of occupied hours above 24°C were below 3%. The results demonstrated that in typical period, there was no overheating in both TLRs. $degree.hours$ in **E220** was on average 335% higher than **E120**. With operation of **NNV** at night, **E120** had lower peak T_{ra} compared to **E220** by 2°C- 5°C.

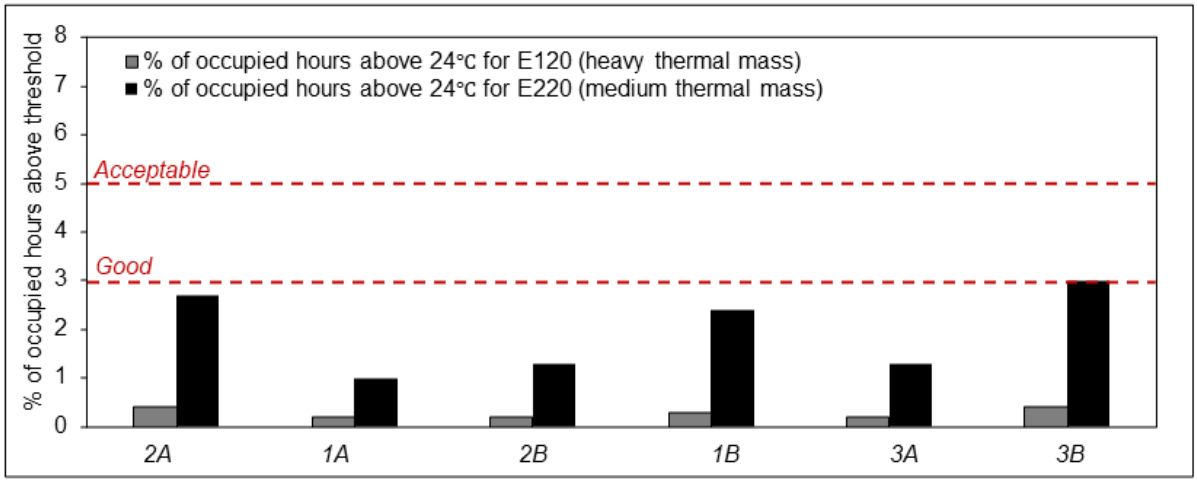

Fig. 10. (%) of occupied hours above a 24°C threshold for **E120** and **E220** for the **NS** case. The corresponding duration in **TMY** (2010s) weather data is the same as the 6-day **HW**

4.2. Impact of increasing doS

Apart from assessing the most critical time of shock occurrence, it is also crucial to understand, how each type of shock impacts the two TLRs while doS increases. To assess the impact of each shock type (**ES** and **SS**), doS was increased from 0 (**NS**) to doS_{max}.

4.2.1. External Shock (ES)

Figure 11 illustrates the evolution of $degree.hours$ for both TLRs for 6 extreme **HW**s (**Table 1)** in increasing $doES_{HW}$ order from $doES_{HW\ min}$ to $doES_{HW\ max.}$ ($\Delta(doES_{HW}) = 0.308$). The impact of the intensity; duration, and severity of **HW**s (**Table 1**) had a significant influence on the $doES_{HW}$. Thus, the mid-term intense **HW** (**ID = 2A**) had the lowest impact on the two TLRs and long-term severe **HW** (**ID = 3B**) had the highest impact. The rate of increase of each $doES_{HW}$ is proportional to the rate of increase of $degree.hours$ in both TLRs. There were significant increase in degree.hours during the **HW**s compared to their respective **NS** scenarios. For **ES**, with $doES_{HW\ min}$. (HW ID = 2A) $degree.hours$ increased by 132× and 6× compared to $degree.hours$ in **NS** scenario for **E120** and **E220** respectively. During $doES_{HW\ max}$. (**HW ID** = **3B**) $degree.hours$ for **E120** and **E220** increased by 36× and 7× respectively compared to $degree.hours$ in **NS** scenario. 100% of the occupied hours were

beyond the 24℃ threshold when the building was evaluated against a $doES_{HW\ max}$. When the duration of **HW** increased from 6 (**ID = 2A**) to 10 days (**ID = 1A**), $doES_{HW}$ increases 2.8× whereas $degree.hours$ increase 1.5× for both TLRs. As the duration and severity of **HW**s increases from 10 days and 18°C.days (**ID = 1A**) to 45 days and 46.1°C.days (**ID = 3B**), $doES_{HW}$ increases by 1.2× for each **HW**, whereas $degree.hours$ increased 1.4× for each **HW**. For **both TLRs,** $doES_{HW\ max}$ had 5× more impact than $doES_{HW\ min}$. During all the HWs, 80% of the occupied hours were above the 24℃ threshold, significantly above the 5% acceptable limits (**Section 2.1**). During **HW**s, **E120** had 1.2× less degree.hours compared to **E220**.

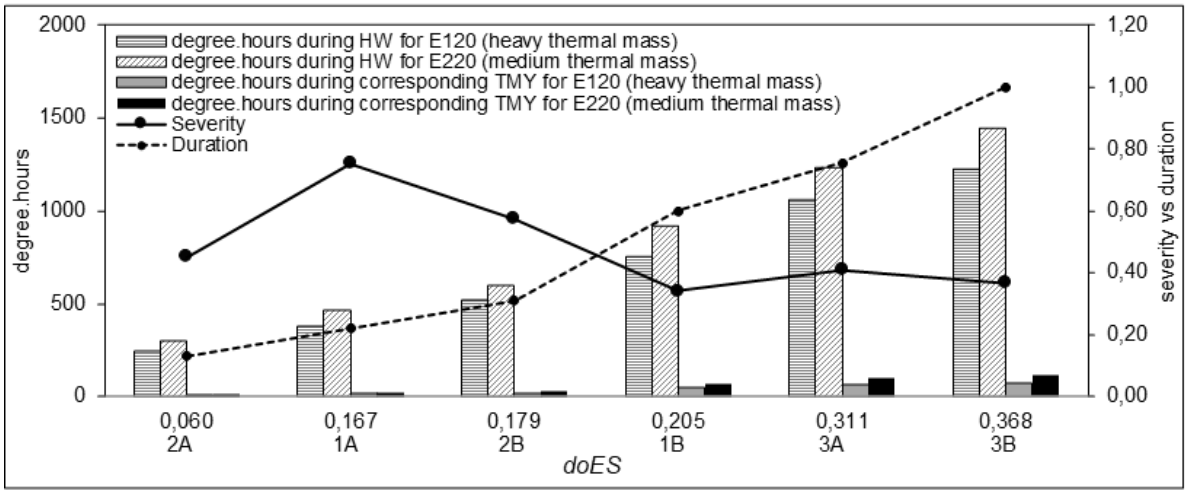

Fig. 11. Comparison of impact of $doES_{HW}$ of 6 extreme HWs for Ghent in **E120** and **E220**

4.2.2. System shocks (SS)

The impact of increasing $doSS$ and varying time of occurrence for **IEC**, **SF** and **NNV** has been illustrated in **Fig. 12**. **Table 2** gives an overview of the different **SS** simulation scenarios. Each **SS** has been increased by a duration of 30 minutes from **NS** to $doSS_{\ max}$.

(a) **Increasing $doSS$:**

If the **IEC** failure occurred from 7:30 a.m. to 6:00 p.m., $degree.hours$ in **E120** and **E220** increased by 5.7× and 4× respectively compared to no **IEC** failure. With the increase in shock duration, the severity of the shock also increased due to heat build-up in the lecture rooms

without cool supply air. $\Delta(doSS_{IEC})$ increased by 2× when shock duration increases from 0' (**NS**) to 30'. Additionally, $\Delta(doSS_{IEC})$ increased by 1.5× for each additional 30' shock from 30' to 180', 1.2× from 180' to 390' and 1.1× increase from 390'to 630'. For each 30' increase in shock duration, $degree.hours$ in both TLRs increased by 1.2×. For **E120**, a 630' **IEC** failure still resulted in less than 6 $degree.hours$. However, for **E220**, 3 hours of **IEC** failure already violated this threshold.

If the **SF** occurred from 1:30 p.m. to 6:00 p.m., $degree.hours$ in both TLRs increased by 4× compared to no **SF**. As duration of **SF** increased, severity of the shock increased due to high solar gains through the envelope. $\Delta(doSS_{SF})$ increased by 1.5× when the shock duration increased from 0' (**NS**) to 30'. Additionally, $\Delta(doSS_{SF})$ increased by 1.1× for each additional 30' shock from 30' to 270'. For each 30' increase in shock duration, $degree.hours$ in both TLRs increased by 1.1×. For **E120**, 270' **SF** still resulted in less than 6 $degree.hours$. However, for **E220**, 45' of **IEC** failure already violated this threshold.

If **NNV** failure occurred from 10:00 p.m. to 6:00 a.m., $degree.hours$ in **E120** and **E220** increased by 4.5× and 3× respectively compared to no **NNV** failure. With increase in shock duration, severity of the shock also increased due to lack of ventilative cooling. Both lecture rooms are unable to flush out the heat build-up during the day due to internal and solar gains. $doSS_{NNV}$ for **E120** was higher than **E220**. For both TLRs, until 120' shock, there was no increment in $doSS_{NNV}$. From 120' to 480', for each additional 30' of **NNV** failure, $\Delta(doSS_{NNV})$ increased by 1.2×. This resulted in 1.3× increase in $degree.hours$ for each 30'. For **E120**, 480' **NNV** failure still resulted in less than 6 $degree.hours$. However, for **E220**, 160'of **NNV** failure already violated this threshold.

(b) **Most critical time of shock occurrence:**

Each **SS** can occur at any time within its operation period. For both TLRs, in the case of **SF**, **IEC and NNV** failures, the highest $degree.hours$ were obtained when the shock

occurred at the start of the operational time of the system (i.e., **IEC** failure at 7:30 a.m., **SF** at 1:30 p.m. and **NNV** failure at 10:00 p.m.). For **IEC** failure, in both TLRs, $degree.hours$ were respectively 1.2× and 1.3× lower when the shock occurred at 9:45 a.m. and 3:00 p.m. instead of 7:30 a.m. It might be noted that until a 270' shock, the most critical time of occurrence was at 9:45 a.m. due to its high occupancy. But due to higher heat build-up in indoor spaces, shock starting at 7:30 a.m. proved to be most critical. For **SF**, in both TLRs, there was an average 1.4× increase in $degree.hours$ when the shock occurred at 1:30 p.m. instead of 3:00 p.m. **NNV** failure occurring at 10:00 p.m. was the most critical time of shock for both TLRs. For example, in **E120**, **NNV** failure at 10:00 p.m., led to 1.2×, 1.1× and 1.5× increase in $degree.hours$ compared to a failure occurring at 12:00 a.m., 2:00 a.m. and 4:00 a.m. respectively.

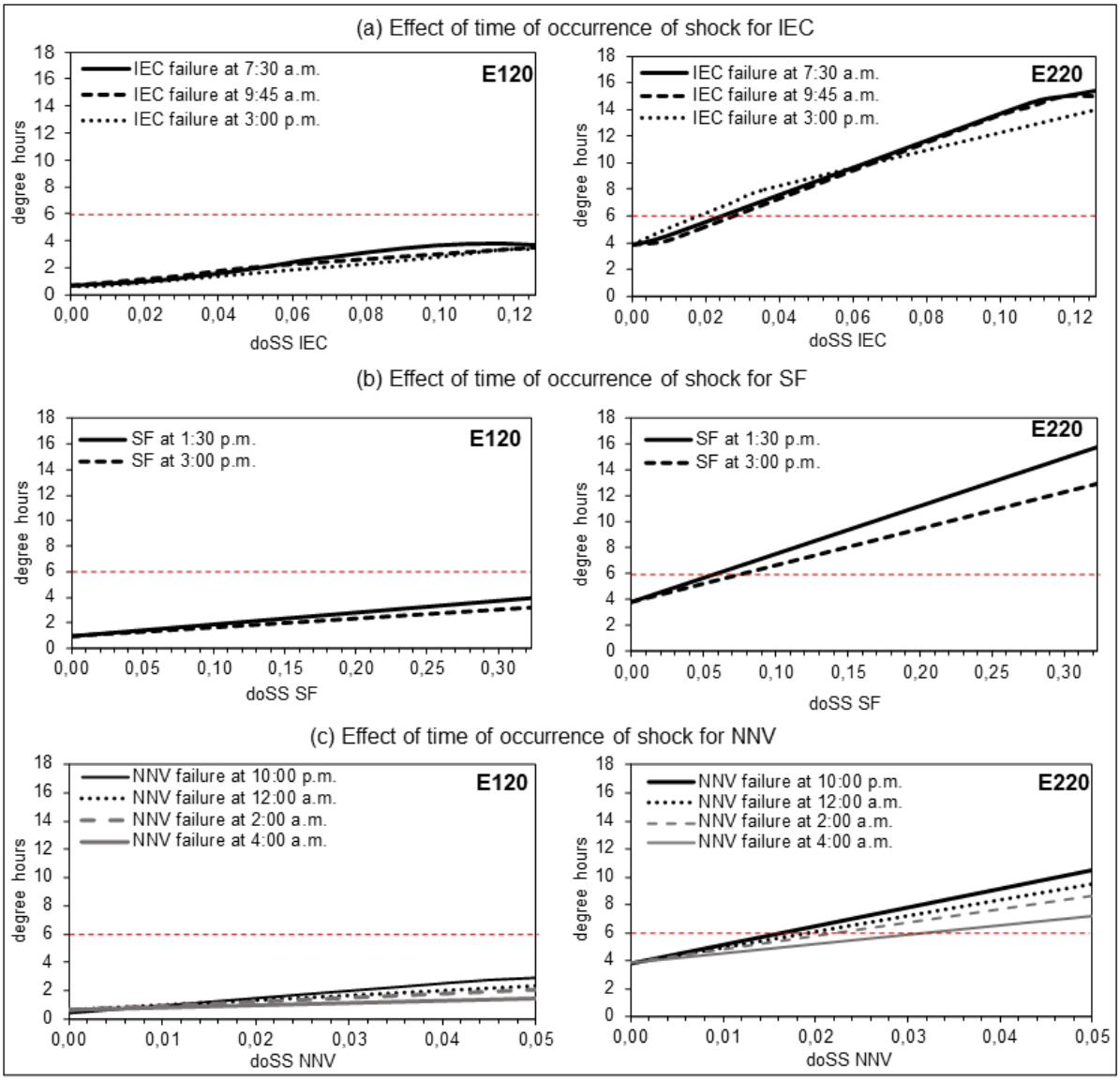

Fig. 12. Impact of **SS** (**IEC, SF** and **NNV**) and corresponding $degree.hours$ for **E120** and **E220**

4.3. Impact of shock combinations

Figure 13 shows the impact of different combinations of **ES (HW, ID = 2A, Table 1**) + **SS (SF, IEC** and **NNV)** failure during the whole operation period and combinations of them at the most critical times of occurrence) and **SS**+**SS** (**Table 3**). The $degree.hours$ for the different **ES**+**SS** and **SS**+**SS** were plotted in increasing order from least to most severe.

According to **Fig. 13b**, in both TLRs, **IEC+SF** resulted in higher $degree.hours$ than **IEC+NNV** failure, followed by **SF+NNV** failure. For example, in **E120**, $degree.hours$ for **IEC+SF** failure were 1.1× higher than **IEC+NNV** and **SF+NNV** failure respectively. Thus

combinations having the least impact are the ones without IEC failure (i.e., lack of cooling). The worst is AHU failure (i.e., lack of cooling and ventilation: no load removal).Combining three **SS** resulted in 3× higher $degree.hours$ than two **SS** except for **IEC+VF**. **IEC+VF+SF** was the most critical followed by **IEC+VF IEC +SF+NN.** For example, in **E120**, $degree.hours$ for **IEC+VF+SF** failure were 1.7× and 2.7× higher than **IEC+VF** and **IEC+SF+NNV** failures respectively. For three combined **SS**, the worst is also the one with AHU failure. Combining all **SS** resulted in the highest $degree.hours$. For example, in **E120**, $degree.hours$ for **IEC**+**VF+SF+NNV** failure were 3.6× higher than those for **IEC+SF+NNV.**

According to **Fig. 13c**, in both TLRs, **HW+IEC** failure resulted in higher $degree.hours$ than **HW+SF**, followed by **HW+NNV** failure. For example, in **E120**, $degree.hours$ for **HW+IEC** failure were 1.1× higher than **HW+SF** and **HW+NNV** failure respectively. Combining two **SS** with the **HW** resulted in 1.3× higher $degree.hours$ than single **SS**+**HW** with **HW+(IEC+SF)** being the most critical followed by **HW+(NNV+SF), HW+(IEC+NNV)** and **HW+(IEC+VF)**. For example, in **E120**, $degree.hours$ for **HW+(IEC**+**SF)** failure were 1.07×, 1.04× and 1.03× higher than **HW+(NNV+SF), HW+(NNV+IEC)** failures and **HW+(IEC+VF)** respectively. Adding an additional **SS** to the **ES+SS** combinations resulted in 1.02× higher $degree.hours$ with **HW+(IEC+SF+VF)** being more critical than **HW+(IEC+SF+NNV).** For example, in **E120**, $degree.hours$ for **HW+(IEC+SF+NNV)** failure were 1.01× higher than **HW+(IEC**+**VF+SF).**

According to **Fig. 13**, combinations of the same number of **ES+SS** were always more critical than those of **SS+SS**. For example, in **E120**, $degree.hours$ for **HW+IEC** failure was 15× higher than **IEC+VF.** The $degree.hours$ for **HW+IEC+SF** was 9.2× higher than **IEC+VF+SF** failure and $degree.hours$ for **HW+IEC+SF+NNV** were 7.1× higher than **IEC+SF+NNV+VF**. Note that the $degree.hours$ in **E220** were always higher than in **E120.**

For example, $degree.hours$ during **HW+IEC+VF+SF+NNV** is 1.1× higher in **E220** than **E120**.

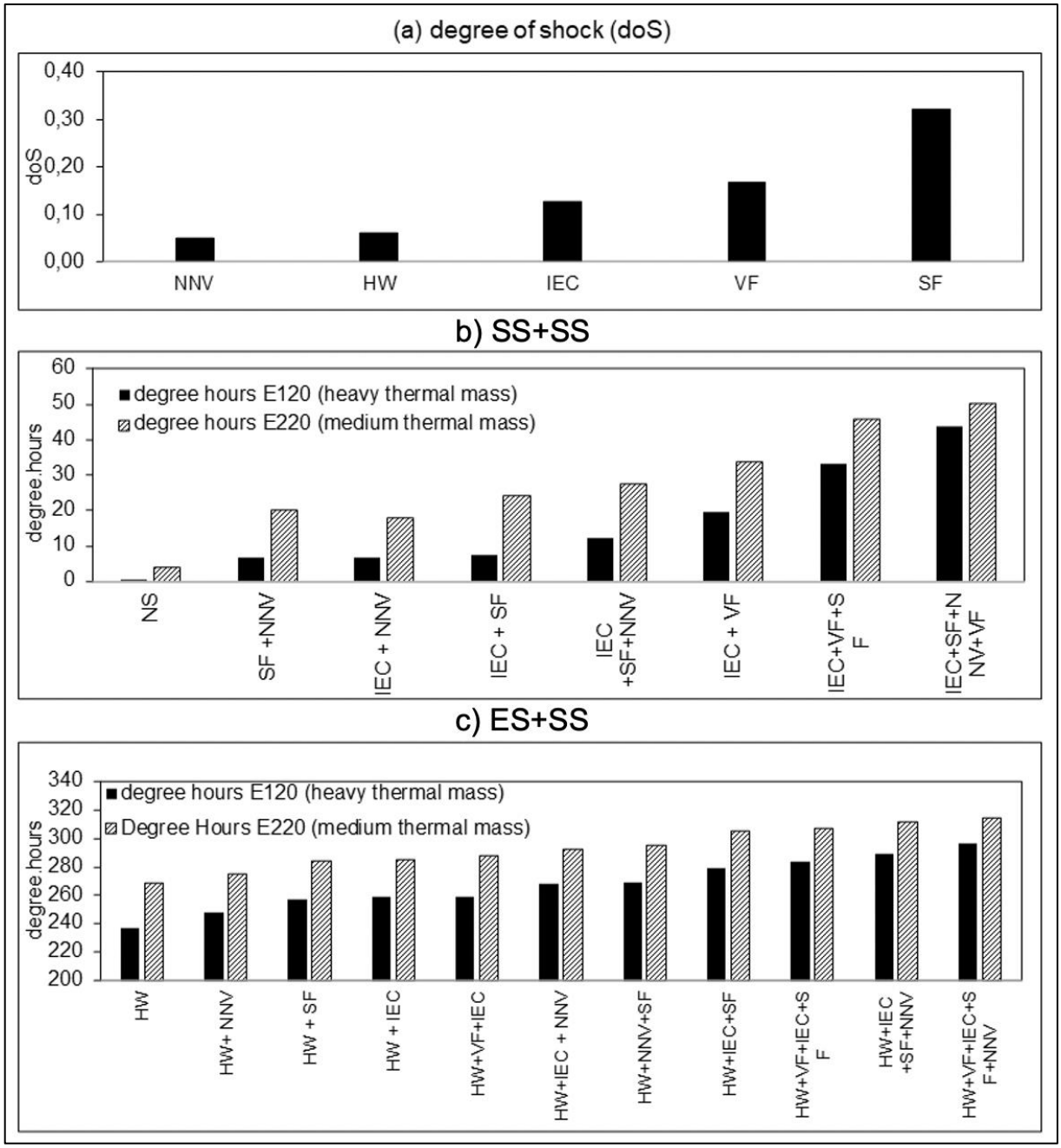

Fig. 13. Effect of combined **SS**+**SS** and **ES**+**SS** shocks on thermal comfort and thermal resilience to overheating in **E120** and **E220**

5. Discussions

5.1 Impact of shocks on nZEB non-residential buildings

Assessing of the impact of **ES** on the two TLRs (section 4.2.1) demonstrated that during **HW**s, combinations of passive cooling strategies working in their full capacity cannot remove excess heat build-up and there was evident overheating in both TLRs. The effectiveness of evaporative coolers relies heavily on the outdoor psychrometric conditions. Since **HW**s result in increased wet bulb and dew point temperatures, the cooling capacity of evaporative coolers (i.e., direct, indirect and dew point evaporative coolers) is significantly reduced. The same applies for strategies that rely on diurnal temperature differences that are extremely reduced during a **HW**. Example of such strategies are **NNV** used in this case study and radiative cooling panels. The same applies for envelope shading strategies, which effectiveness reduces considerably with increased solar irradiation on windows during **HW**s. Note that for **NNV**, its effectiveness not only relies on diurnal temperature gradients but also on the design, favourable wind directions and velocities, window opening area. To be maximally efficient, **NNV** relies on stack effect establishment. This is not the case in the current case study building. Moreover, the windows' opening area was limited to 8°.

Failure of different systems proved that they deliver their highest cooling efficiency at the beginning of their operational period as they don't allow for significant heat to build up inside the space. For example, if the **IEC** failure was to occur later at 9:45 a.m. or 3:00 p.m., TLRs would have been partially cooled by the **IEC** since the start of its operation in the morning until a failure occurred. The decrease in the occupancy during break would also contribute to lower violations. **SF** occurring later throughout the day would protect the space from the highest solar irradiation at noon. If the **NNV** failure would have occurred at a later period, the partial operation of **NNV** from 10:00 p.m., until the time of occurrence of the shock would have already ventilated the two TLRs, lowering the $\overline{T_{ra\ E120}}$ and $\overline{T_{ra\ E220}}$.

5.2 Comparison of different shock types

To compare the different shock types, a common range of doS for **ES** and **SS** was chosen. A common doS range of [0- 0.368] was selected. For ES this corresponds to the different HWs defined in **Table 1**. For an IEC-SS, this corresponds to 0 to 3 days failure for E120 and 0 to 5 days for E220. Similarly for SF-SS this corresponds to 0 to 1.5 days failure for E120 and 0 to 3 days for E220. For NNV-SS this corresponds to 0 to 12 nights failure for E120 and 0 to 18 nights for E220. **Figure 14** compares the impact of the same doS on the two TLRs due to different shock types. According to **Fig. 14**, across the entire doS range and for both TLRs, **ES** was more critical than all **SS** types by several orders of magnitude. For **SS**, **NNV** failure was the most critical followed by **IEC** failure and **SF**. For example, in **E120**, for $doS = 0.368$, **ES** resulted in 110× higher $degree.hours$ compared to **IEC** failure, 290× higher than **SF** and 31× higher than *i***NNV** failure. Similarly, for **E220**, for $doS = 0.368$, **ES** resulted in 43× higher $degree.hours$ than **IEC** failure, 75× higher than **SF** and 22× higher than **NNV** failure. This also explains why during shock combinations, any **ES+SS** was more critical than **SS+SS** (**Fig. 13**).

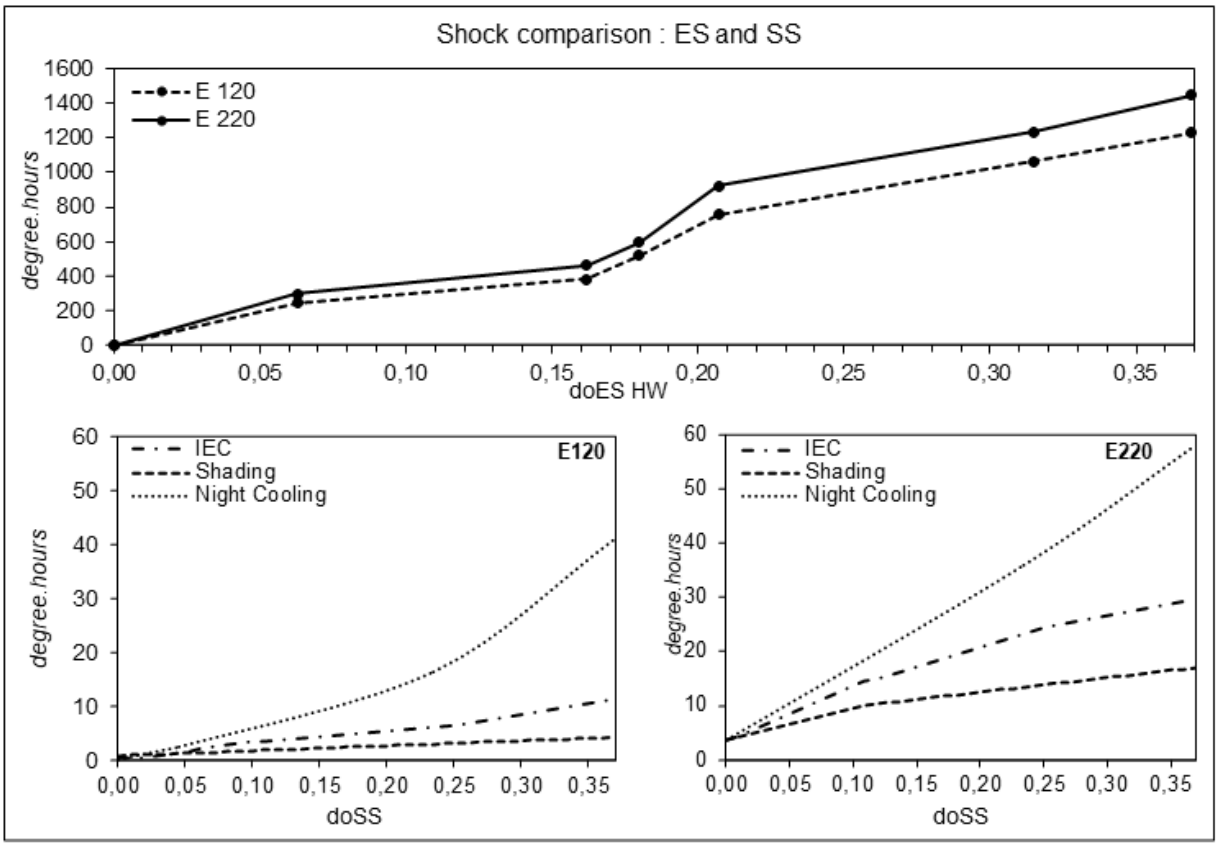

Fig. 14. Comparison of the effect of **ES**, and **SS** in **E120** and **E220**

5.3 Impact of thermal mass

The results showed that during the case of **NS** and during the cases of **ES** and **SS** as well as combinations of them, the temperature violations in **E220** were higher than in **E120**. Comparing both classrooms, this can be since **E220** has a lighter thermal mass than **E120**. However, it can also be since **E220** has higher heat gains due to the presence of the roof. However, despite having the same number of average occupants over the week (32 occupants in **E120** and 34 occupants in **E220**), the number of occupied hours in **E120** was higher than **E220** (35 h vs 19 h for **E120** and **E220** respectively). Thus, conclusions on the impact of thermal mass cannot be immediately drawn and the two classrooms cannot be compared. Additional simulations were conducted where the thermal mass was varied in each classroom between light brick (ρ = 850 kg/m^3), medium brick (ρ = 1400 kg/m^3), and heavy brick (ρ = 1850 kg/m^3). The specific capacity of the different bricks remained the same (C_p = 840 J/kg.K). The brick was

located at the interior layer of the building envelope wall in E120. The rest of the parameters were not varied.

The simulations were conducted for the case of No shock (**NS**), and the case of an **ES** as they are the worst types of shock when compared to **SS**. The **HW** (**ID = 2A**, **Table 1**) was again selected (as justified in section 3.4.3). **Figure 15** illustrates the degree hours and temporal temperature profile in **E120** for a) **NS** and b) **HW** for light, medium and heavy thermal mass. Results showed that both for the cases of **NS** and **HW**, increasing the thermal mass density from light to heavy reduced the room air temperatures during the day and thus reduced the unmet cooling degree.hours. This is since the heavier thermal mass was able to store more thermal energy, providing inertia against temperature fluctuations. However, the damping efficiency of the thermal mass was reduced in the **HW** scenario as compared to **NS**. For example in **E120**, for the case of **NS**, the degree.hours decreased by 32.4% when switching from light to medium thermal mass and further by 20% when switching to a heavy thermal mass. However, during a **HW**, the degree.hours decreased by 7% when switching from light to medium thermal mass and further by 4.7% when switching to a heavy thermal mass. This can be due to the extremely high outdoor temperatures during both night-time and daytime encountered during a **HW** and the reduction in diurnal temperature differences.

The damping efficiency of thermal mass was also less pronounced due to its higher heat gains from the roof. For the case of **NS**, the degree.hours decreased by 21.7% when switching from light to medium thermal mass and further by 14.2% when switching to a heavy thermal mass. During a **HW**, the degree.hours decreased by 6.3% when switching from light to medium thermal mass and further by 4% when switching to a heavy thermal mass. Thus, the thermal mass has an impact on the thermal resilience performance of nZEB during overheating events, however less pronounced than during reference scenarios with NS. The discrepancies found

between the classrooms can be attributed in part to the thermal mass but also to the increased solar gains in **E220** given the presence of the roof.

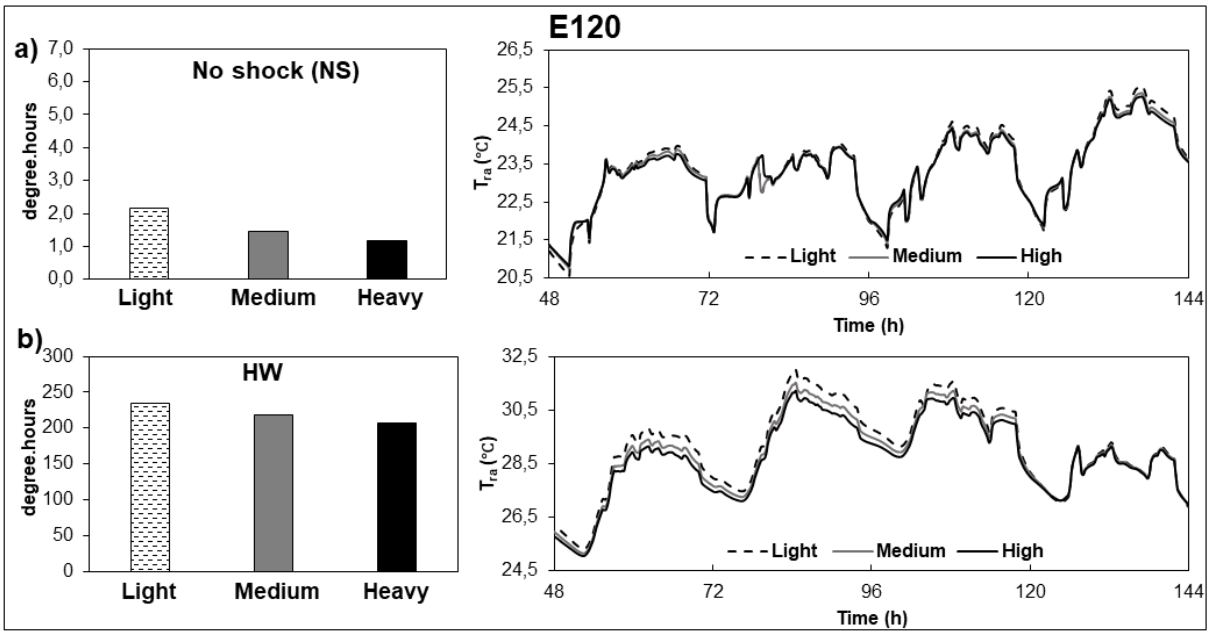

Fig. 15. Illustration of the degree.hours (left) and temporal room air temperature variation (right) for different thermal mass for the case of a) no shock (NS) and b) HW (ID=2A) for E120

6. Conclusions

In this work, doS was introduced to classify, quantify and compare the impact of different shock types on the thermal resilience to overheating in two lecture rooms. The key conclusions were summarized below:

- Impact of shock types: The impact of **ES** (in this study **HW**s) is significantly higher than any **SS**. **HW**s in future climate scenarios can be considered as the most extreme shock for nZEB buildings. HWs impact the outdoor climate conditions by simultaneously increasing dry bulb, wet bulb, and dew point temperatures as well as solar gains. They also reduce the diurnal differences in ambient air temperatures between day and night. HWs will not only significantly increase envelope gains but renders inefficient passive cooling strategies which performance relies on ambient

outdoor conditions. Thus, shock combinations with HW which will become more frequent in future scenarios will also be the most critical.

- To assess buildings' resilience to overheating against **ES**, different **HW**s should be assessed (e.g., short and intense which will impact the absorptivity of the shock or long and severe which will impact the recovery of the shock). In long-term future, as HWs get longer in duration and higher in intensity, the buildings' thermal resilience to overheating is compromised and the passive cooling strategies fail to remove the heat build-up in the indoor space during **HW**s.
- The time lag effect of thermal mass in nZEB diminishes during HWs. Thus, thermal mass doesn't improve the thermal resilience performance of nZEB during HWs, as is the case during typical conditions. The discrepancies found between the classrooms can be attributed in part to the thermal mass but mostly to the increased solar gains in **E220** given the presence of the roof.

7. Limitations and outlook

This methodology developed in this paper for classifying and quantifying **ES** and **SS** is applicable to any type of building equipped with any type of cooling strategy, with knowledge of (a) weather data and (b) occupancy profiles. For **ES**, only **HW**s have been investigated. However, there is a growing need to include the impact of urban heat island effect in the weather data to assess the severity of overheating risk in buildings in an urban context. On the other hand, this study assessed the impact of shocks on the thermal resilience of a nZEB building using the $degree.hours$ and the % of occupied hours. However, such indicators do not give insight into the other resilience aspects (i.e., **absorptivity** and **recovery**). Thus, there is a need to develop a holistic resilience performance indicator and the current study is the first step towards this goal. Future work will sensitivity analysis to evaluate the most influential building

and system design parameters that impact the thermal resilience to overheating. Other building typologies and associated systems will be investigated. Together with the doS, this can establish a quantitative assessment framework that can be used to test and improve resilience to overheating in todays' buildings and systems.

Note that this method can be applied in any resilience domain, where shocks can be characterized by their severity (i.e., variable responsible for shock occurrence) and duration, thus posing a threat to the performance of an engineered system. The doS can thus be used to quantify the shocks, compare their impact on system performance and adopt mitigating strategies. Examples include building construction resilience during the occurrence of natural disasters (i.e., earthquakes, fire, flooding). The doS can be expressed in terms of the change in loading on the building foundation and the duration of the disturbance.

Acknowledgements

This study is performed under the framework of International Energy Agency's Energy in Buildings and Communities (IEA EBC) Annex 80 - Resilient Cooling of Buildings. This work has been supported by the Flanders Innovation and Entrepreneurship in the Flux 50 Project 'ReCOver++: Improving resilience of buildings to overheating.'

References

[1] G. Lamberti, G. Salvadori, F. Leccese, F. Fantozzi, P.M. Bluyssen, M.K. Singh, sustainability Advancement on Thermal Comfort in Educational Buildings: Current Issues and Way Forward Academic Editors: Mitja Košir and, (2021). https://doi.org/10.3390/su131810315.

[2] M. Fonseca Gabriel, I. Paciência, F. Felgueiras, J. Cavaleiro Rufo, F. Castro Mendes, M. Farraia, Z. Mourão, A. Moreira, E. de Oliveira Fernandes, Environmental quality in primary schools and related health effects in children. An overview of assessments conducted in the Northern Portugal, Energy Build. 250 (2021) 111305. https://doi.org/10.1016/j.enbuild.2021.111305.

[3] Z.S. Zomorodian, M. Tahsildoost, M. Hafezi, Thermal comfort in educational buildings: A review article, (n.d.). https://doi.org/10.1016/j.rser.2016.01.033.

[4] P. de Wilde, D. Coley, The implications of a changing climate for buildings, Build. Environ. 55 (2012) 1–7. https://doi.org/10.1016/j.buildenv.2012.03.014.

[5] European Green Deal 2019, Antimicrob. Agents Chemother. 58 (2019) 7250–7.

https://doi.org/10.1128/AAC.03728-14.
[6] European Commission, Going climate-neutral by 2050, Facilities. (2018).
[7] S.B. Sadineni, S. Madala, R.F. Boehm, Passive building energy savings: A review of building envelope components, Renew. Sustain. Energy Rev. 15 (2011) 3617–3631. https://doi.org/10.1016/j.rser.2011.07.014.
[8] C.A. Balaras, K. Droutsa, A.A. Argiriou, D.N. Asimakopoulos, Potential for energy conservation in apartment buildings, Energy Build. 31 (2000) 143–154. https://doi.org/10.1016/S0378-7788(99)00028-6.
[9] B. Raji, M.J. Tenpierik, A. Van Den Dobbelsteen, An assessment of energy-saving solutions for the envelope design of high-rise buildings in temperate climates: A case study in the Netherlands, Energy Build. 124 (2016) 210–221. https://doi.org/10.1016/j.enbuild.2015.10.049.
[10] L.G. Valladares-Rendón, G. Schmid, S.L. Lo, Review on energy savings by solar control techniques and optimal building orientation for the strategic placement of façade shading systems, Energy Build. 140 (2017) 458–479. https://doi.org/10.1016/j.enbuild.2016.12.073.
[11] M. Santamouris, D. Kolokotsa, Passive cooling dissipation techniques for buildings and other structures: The state of the art, Energy Build. 57 (2013) 74–94. https://doi.org/10.1016/j.enbuild.2012.11.002.
[12] IEA/EBC, Ventilative Cooling (State-of-the-art review) Annex 62, IEA - EBC Program. Annex 62 (2015) 213. http://venticool.eu/wp-content/uploads/2013/09/SOTAR-Annex-62-FINAL.pdf.
[13] M. Steeman, A. Janssens, M. De Paepe, Performance evaluation of indirect evaporative cooling using whole-building hygrothermal simulations, Appl. Therm. Eng. 29 (2009) 2870–2875. https://doi.org/10.1016/j.applthermaleng.2009.02.004.
[14] OECD/IEA, The Future of Cooling Opportunities for energy-efficient air conditioning Together Secure Sustainable, (2018) 92. www.iea.org/t&c/.
[15] R. Becker, I. Goldberger, M. Paciuk, Improving energy performance of school buildings while ensuring indoor air quality ventilation, Build. Environ. 42 (2007) 3261–3276. https://doi.org/10.1016/j.buildenv.2006.08.016.
[16] C. Heracleous, A. Michael, Assessment of overheating risk and the impact of natural ventilation in educational buildings of Southern Europe under current and future climatic conditions, Energy. 165 (2018) 1228–1239. https://doi.org/10.1016/j.energy.2018.10.051.
[17] J.P. Harrouz, K. Ghali, N. Ghaddar, Integrated solar – Windcatcher with dew-point indirect evaporative cooler for classrooms, Appl. Therm. Eng. 188 (2021) 116654. https://doi.org/10.1016/j.applthermaleng.2021.116654.
[18] S. Homaei, M. Hamdy, Thermal resilient buildings: How to be quantified? A novel benchmarking framework and labelling metric, Build. Environ. 201 (2021) 108022. https://doi.org/10.1016/j.buildenv.2021.108022.
[19] S. Attia, R. Levinson, E. Ndongo, P. Holzer, O. Berk Kazanci, S. Homaei, C. Zhang, B.W. Olesen, D. Qi, M. Hamdy, P. Heiselberg, Resilient cooling of buildings to protect against heat waves and power outages: Key concepts and definition, Energy Build. 239 (2021) 110869. https://doi.org/10.1016/j.enbuild.2021.110869.
[20] A. Laouadi, M. Bartko, A. Gaur, M.A. Lacasse, Climate Resilience Buildings : Guideline for management of overheating risk in residential buildings, (2021).
[21] J. Hassi, M. Rytkönen, J. Kotaniemi, H. Rintamäki, Impacts of cold climate on human heat balance, performance and health in circumpolar areas., Int. J. Circumpolar Health. 64 (2005) 459–467. https://doi.org/10.3402/ijch.v64i5.18027.
[22] Africa Research Institute, Between extremes, 123 (2012) 275–280.

[23] B.G. Armstrong, Z. Chalabi, B. Fenn, S. Hajat, S. Kovats, A. Milojevic, P. Wilkinson, Association of mortality with high temperatures in a temperate climate: England and Wales, J. Epidemiol. Community Health. 65 (2011) 340–345. https://doi.org/10.1136/jech.2009.093161.
[24] R. Vautard, A. Gobiet, S. Sobolowski, E. Kjellström, A. Stegehuis, P. Watkiss, T. Mendlik, O. Landgren, G. Nikulin, C. Teichmann, D. Jacob, The European climate under a 2 °c global warming, Environ. Res. Lett. 9 (2014). https://doi.org/10.1088/1748-9326/9/3/034006.
[25] C. Hughes, S. Natarajan, Summer thermal comfort and overheating in the elderly, Build. Serv. Eng. Res. Technol. 40 (2019) 426–445. https://doi.org/10.1177/0143624419844518.
[26] C. Sigauke, M.M. Nemukula, Modelling extreme peak electricity demand during a heatwave period: a case study, Energy Syst. 11 (2020) 139–161. https://doi.org/10.1007/s12667-018-0311-y.
[27] A. Golub, K. Govorukha, P. Mayer, D. Rübbelke, Climate Change and the Vulnerability of Germany's Power Sector to Heat and Drought, Energy J. 43 (2022) 157–184. https://doi.org/10.5547/01956574.43.3.agol.
[28] R. Vautard, O. Boucher, P.) Geert, J. Van Oldenborgh, F. Otto, K. Haustein, M.M. Vogel, S.I. Seneviratne, J.-M. Soubeyroux, M. Schneider, A. Drouin, Human contribution to the record-breaking July 2019 heat wave in Western Europe, World Weather Attrib. (2019). https://public.wmo.int/en/media/news/july-heatwave-has-multiple-impacts.
[29] 2019 | HUMAN WRONGS WATCH, (n.d.). https://human-wrongs-watch.net/2019/ (accessed October 21, 2022).
[30] A. Sengupta, P. Proot, T. Trioen, H. Breesch, M. Steeman, Impact of future climate on the performances of ground-source cooling system, CLIMA 2022 Conf. (2022). https://doi.org/10.34641/CLIMA.2022.326.
[31] Z. De Grussa, D. Andrews, G. Lowry, E.J. Newton, K. Yiakoumetti, A. Chalk, D. Bush, A London residential retrofit case study: Evaluating passive mitigation methods of reducing risk to overheating through the use of solar shading combined with night-time ventilation, Build. Serv. Eng. Res. Technol. 40 (2019) 389–408. https://doi.org/10.1177/0143624419840768.
[32] J. Verhelst, G. Van Ham, D. Saelens, L. Helsen, Economic impact of persistent sensor and actuator faults in concrete core activated office buildings, Energy Build. 142 (2017) 111–127. https://doi.org/10.1016/j.enbuild.2017.02.052.
[33] X. Lu, Z. O'Neill, Y. Li, F. Niu, A novel simulation-based framework for sensor error impact analysis in smart building systems: A case study for a demand-controlled ventilation system, Appl. Energy. 263 (2020) 114638. https://doi.org/10.1016/j.apenergy.2020.114638.
[34] C.Y. Leong, Fault Detection and Diagnosis of Air Handling Unit: A Review, MATEC Web Conf. 255 (2019) 06001. https://doi.org/10.1051/matecconf/201925506001.
[35] F.M. Baba, H. Ge, L. (Leon) Wang, R. Zmeureanu, Do high energy-efficient buildings increase overheating risk in cold climates? Causes and mitigation measures required under recent and future climates, Build. Environ. 219 (2022) 109230. https://doi.org/10.1016/j.buildenv.2022.109230.
[36] F. Shi, Z. Lin, Q. Li, O.E. Ozbulut, Z. He, Y. Zhou, Design, manufacturing, and testing of a hybrid self-centering brace for seismic resilience of buildings, Earthq. Eng. Struct. Dyn. (2023) 1–22. https://doi.org/10.1002/eqe.3821.
[37] W. Liu, K. Ikago, Performance of a passive rate-independent damping device in a seismically isolated multistory building, Struct. Control Heal. Monit. 29 (2022) 1–22.

https://doi.org/10.1002/stc.2941.
[38] M. Gravit, D. Shabunina, S. Antonov, A. Danilov, Thermal Characteristics of Fireproof Plaster Compositions in Exposure to Various Regimes of Fire, Buildings. 12 (2022). https://doi.org/10.3390/buildings12050630.
[39] S. Gawdat, A. Farouk, A. Farid, THE USE OF NANO-GLASS IN PASSIVE FIRE SAFETY IN BUILDINGS 225–218) 2023(16, صخلملا.
[40] IEA EBC || Annex 80 || Resilient Cooling, (n.d.). http://annex80.iea-ebc.org/ (accessed February 28, 2020).
[41] E. Tavakoli, A. O'Donovan, M. Kolokotroni, P.D. O'Sullivan, Evaluating the indoor thermal resilience of ventilative cooling in non-residential low energy buildings: A review, Build. Environ. 222 (2022) 109376. https://doi.org/10.1016/j.buildenv.2022.109376.
[42] L. Ji, C. Shu, A. Laouadi, M. Lacasse, Pr ep rin t n er r iew Pr ep rin t n ed, (n.d.).
[43] A. Sengupta, H. Breesch, D. Al Assaad, M. Steeman, Evaluation of thermal resilience in a case study building during future heatwaves and power outages, (2022).
[44] A. Sengupta, M. Steeman, H. Breesch, Analysis of Resilience of Ventilative Cooling Technologies in a Case Study Building, ICRBE Procedia. (2020). https://doi.org/10.32438/iCRBE.202041.
[45] M. Atrigna, A. Buonanno, R. Carli, G. Cavone, P. Scarabaggio, M. Valenti, G. Graditi, M. Dotoli, Effects of Heatwaves on the Failure of Power Distribution Grids: A Fault Prediction System Based on Machine Learning, 21st IEEE Int. Conf. Environ. Electr. Eng. 2021 5th IEEE Ind. Commer. Power Syst. Eur. EEEIC / I CPS Eur. 2021 - Proc. (2021). https://doi.org/10.1109/EEEIC/ICPSEurope51590.2021.9584751.
[46] The Modelica Association — Modelica Association, (n.d.). https://www.modelica.org/ (accessed June 8, 2020).
[47] A. Moazami, S. Carlucci, S. Geving, Robust and resilient buildings: A framework for defining the protection against climate uncertainty, (n.d.). https://doi.org/10.1088/1757-899X/609/7/072068.
[48] A.C. Van Der Linden, A.C. Boerstra, A.K. Raue, S.R. Kurvers, R.J. De Dear, Adaptive temperature limits: A new guideline in the Netherlands: A new approach for the assessment of building performance with respect to thermal indoor climate, Energy Build. 38 (2006) 8–17. https://doi.org/10.1016/j.enbuild.2005.02.008.
[49] Q. Zhao, Z. Lian, D. Lai, Thermal comfort models and their developments: A review, Energy Built Environ. 2 (2021) 21–33. https://doi.org/10.1016/j.enbenv.2020.05.007.
[50] L. Toledo, P. Cropper, A.J. Wright, Vulnerability and resilience in energy efficient homes : thermal response to heat waves, in: PLEA2017_proceedings_volume_I, PLEA, 2017: pp. 875–902. https://plea2017.net/ (accessed February 28, 2020).
[51] N. Torabi, H.B. Gunay, W. O'Brien, T. Barton, Common human errors in design, installation, and operation of VAV AHU control systems – A review and a practitioner interview, Build. Environ. 221 (2022) 109333. https://doi.org/10.1016/j.buildenv.2022.109333.
[52] T. Leenanunath, N. Sirivongpaisal, Energy management by simulation of air handling unit degradation behavior for planning maintenance schedule, ICMIT 2006 Proc. - 2006 IEEE Int. Conf. Manag. Innov. Technol. 2 (2006) 1070–1074. https://doi.org/10.1109/ICMIT.2006.262387.
[53] K. Sun, W. Zhang, Z. Zeng, R. Levinson, M. Wei, T. Hong, Passive cooling designs to improve heat resilience of homes in underserved and vulnerable communities, Energy Build. 252 (2021) 111383. https://doi.org/10.1016/J.ENBUILD.2021.111383.
[54] B.W. Olesen, Revision of EN 15251: Indoor Environmental Criteria: REHVA, 2012. http://www.rehva.eu/publications-and-resources/hvac-journal/2012/042012/revision-

of-en-15251-indoor-environmental-criteria/.
[55] TM52: The Limits of Thermal Comfort: Avoiding Overheating in European Buildings | CIBSE, (n.d.). https://www.cibse.org/knowledge-research/knowledge-portal/tm52-the-limits-of-thermal-comfort-avoiding-overheating-in-european-buildings (accessed November 15, 2022).
[56] EN 16798-1:2019 - Energy performance of buildings - Ventilation for buildings - Part 1: Indoor, (n.d.). https://standards.iteh.ai/catalog/standards/cen/b4f68755-2204-4796-854a-56643dfcfe89/en-16798-1-2019 (accessed December 9, 2021).
[57] Menerga | Menerga, (n.d.). https://www.menerga.com/ (accessed June 29, 2022).
[58] Passive House Definition Independent of Climate, (n.d.). https://web.archive.org/web/20121005015936/http://www.passivhaustagung.de/Passive_House_E/passivehouse_definition.html (accessed June 29, 2022).
[59] Search results standards: NBN EN ISO 13790 | NBN Shop, (n.d.). https://www.nbn.be/shop/en/search/?k= NBN EN ISO 13790&y=&ics= (accessed November 23, 2021).
[60] B. Merema, M. Delwati, M. Sourbron, H. Breesch, Demand controlled ventilation (DCV) in school and office buildings: Lessons learnt from case studies, Energy Build. 172 (2018) 349–360. https://doi.org/10.1016/J.ENBUILD.2018.04.065.
[61] B. Merema, D. Saelens, H. Breesch, Demonstration of an MPC framework for all-air systems in non-residential buildings, Build. Environ. 217 (2022) 109053. https://doi.org/10.1016/j.buildenv.2022.109053.
[62] H. Breesch, B. Merema, A. Versele, Ventilative Cooling in a School Building : Evaluation of the Measured Performances, (2018). https://doi.org/10.3390/fluids3040068.
[63] Dymola - Dassault Systèmes®, (n.d.). https://www.3ds.com/products-services/catia/products/dymola/ (accessed July 18, 2022).
[64] F. Jorissen, G. Reynders, R. Baetens, D. Picard, D. Saelens, L. Helsen, Implementation and verification of the ideas building energy simulation library, J. Build. Perform. Simul. 11 (2018) 669–688. https://doi.org/10.1080/19401493.2018.1428361.
[65] K. Ahmed, J. Kurnitski, B. Olesen, Data for occupancy internal heat gain calculation in main building categories, Data Br. 15 (2017) 1030–1034. https://doi.org/10.1016/j.dib.2017.10.036.
[66] Acurity | Personentelling - Camerabewaking - Artikelbeveiliging, (n.d.). https://www.acurity.be/ (accessed July 18, 2022).
[67] D. Al Assaad, C. Habchi, K. Ghali, N. Ghaddar, Simplified model for thermal comfort, IAQ and energy savings in rooms conditioned by displacement ventilation aided with transient personalized ventilation, Energy Convers. Manag. 162 (2018) 203–217. https://doi.org/10.1016/j.enconman.2018.02.033.
[68] D. Al Assaad, A. Sengupta, H. Breesch, Demand-controlled ventilation in educational buildings: Energy efficient but is it resilient?, Build. Environ. 226 (2022) 109778. https://doi.org/10.1016/j.buildenv.2022.109778.
[69] CO2, Temperature and Humidity Transmitter Series GMW90 for green building projects | Vaisala, (n.d.). https://www.vaisala.com/en/products/instruments-sensors-and-other-measurement-devices/instruments-industrial-measurements/gmw90 (accessed July 15, 2022).
[70] M. Borrelli, B. Merema, F. Ascione, R. Francesca De Masi, G. Peter Vanoli, H. Breesch, Evaluation and optimization of the performance of the heating system in a nZEB educational building by monitoring and simulation, Energy Build. 231 (2021) 110616. https://doi.org/10.1016/j.enbuild.2020.110616.
[71] N. Jain, E. Burman, S. Stamp, D. Mumovic, M. Davies, Cross-sectoral assessment of the

performance gap using calibrated building energy performance simulation, Energy Build. 224 (2020) 110271. https://doi.org/10.1016/j.enbuild.2020.110271.
[72] G. Ouzeau, J.M. Soubeyroux, M. Schneider, R. Vautard, S. Planton, Heat waves analysis over France in present and future climate: Application of a new method on the EURO-CORDEX ensemble, Clim. Serv. 4 (2016) 1–12. https://doi.org/10.1016/j.cliser.2016.09.002.
[73] News || IEA EBC || Annex 80, (n.d.). https://annex80.iea-ebc.org/news (accessed November 4, 2022).
[74] A. Machard, C. Inard, J.-M. Alessandrini, C. Pelé, J. Ribéron, A Methodology for Assembling Future Weather Files including Heatwaves for Building Thermal Simulations from Regional Climate Models Multi-years Datasets, Submitt. to Energies. (2020) 1–34.
[75] KMI - Hittegolf, (n.d.). https://www.meteo.be/nl/info/weerwoorden/hittegolf (accessed November 1, 2022).
[76] Belgium starts hottest week of 2022, first real heatwave expected, (n.d.). https://www.brusselstimes.com/268624/belgium-starts-hottest-week-of-2022-first-real-heatwave-expected (accessed November 1, 2022).